Article

Current Biology

PITX2 expression and Neanderthal introgression in *HS3ST3A1* contribute to variation in tooth dimensions in modern humans

Highlights

- Genome-wide association identifies variants impacting dental crown dimensions
- *EDAR* variants affect tooth dimensions following an anterior-posterior gradient
- Variants in *PITX2* and *HS3ST3A1* regulate gene expression during tooth development
- Associated variants in *HS3ST3A1* were introgressed from Neanderthals

Authors

Qing Li, Pierre Faux, Emma Wentworth Winchester, ..., Miguel Delgado, Kaustubh Adhikari, Andrés Ruiz-Linares

Correspondence

medelgado@fcnym.unlp.edu.ar (M.D.), k.adhikari@ucl.ac.uk (K.A.), a.ruizlin@ucl.ac.uk (A.R.-L.)

In brief

Tooth morphology varies through evolution and in modern human populations, but little is known about the genetics of this variation. Li et al. identify genes associated with tooth crown dimensions and expressed during dental development. Variants in one gene stem from Neanderthal, suggesting their role in human dental evolution.

Li et al., 2025, Current Biology *35*, 131–144
January 6, 2025
https://doi.org/10.1016/j.cub.2024.11.027

CellPress

Current Biology

CellPress
OPEN ACCESS

Article

PITX2 expression and Neanderthal introgression in *HS3ST3A1* contribute to variation in tooth dimensions in modern humans

Qing Li,[1,2,26] Pierre Faux,[3,4,27] Emma Wentworth Winchester,[5] Guangrui Yang,[1,6] Yingjie Chen,[1] Luis Miguel Ramírez,[7] Macarena Fuentes-Guajardo,[8] Lauriane Poloni,[9,10] Emilie Steimetz,[9] Rolando Gonzalez-José,[11] Victor Acuña,[12]

(Author list continued on next page)

[1]Ministry of Education Key Laboratory of Contemporary Anthropology and Collaborative Innovation Center of Genetics and Development, School of Life Sciences and Human Phenome Institute, Fudan University, 825 Zhangheng Road, Pudong District, Shanghai 200433, China
[2]State Key Laboratory of Complex Severe and Rare Diseases, Department of Orthopedic Surgery, Peking Union Medical College Hospital, Peking Union Medical College, and Chinese Academy of Medical Sciences, No.1 Shuaifuyuan Wangfujing, Dongcheng District, Beijing 100730, China
[3]Aix-Marseille Université, CNRS, EFS, ADES, 27 Boulevard Jean Moulin, Marseille 13005, France
[4]GenPhySE Université de Toulouse, INRAE, ENVT, 24 Chemin de Borde Rouge, 31326 Castanet Tolosan, France
[5]Department of Genetics and Genome Sciences, University of Connecticut Health, 400 Farmington Avenue, Farmington, CT 06030, USA
[6]Exchange, Development & Service Center for Science & Technology Talents, Sanlihe Road, Beijing 100045, P.R. China
[7]Facultad de Odontología, Universidad de Antioquia, Calle 64 N.º 52-59 Of. 107. Apartado Postal 1226, Medellín, Colombia
[8]Departamento de Tecnología Médica, Facultad de Ciencias de la Salud, Universidad de Tarapacá, Avenida 18 de Septiembre 2222, Arica 1000000, Chile
[9]Biogéosciences, UMR 6282 CNRS, Université de Bourgogne, Dijon 21000, France
[10]EPHE, PSL University, Paris 75014, France
[11]Instituto Patagónico de Ciencias Sociales y Humanas, Centro Nacional Patagónico, CONICET, U9129ACD Puerto Madryn, Argentina
[12]Unidad de Genómica de Poblaciones Aplicada a la Salud, Facultad de Química, UNAM-Instituto Nacional de Medicina Genómica, México City 4510, México
[13]Departamento de Genética, Universidade Federal do Rio Grande do Sul, 90040-060 Porto Alegre, Brasil
[14]Laboratorios de Investigación y Desarrollo, Facultad de Ciencias y Filosofía, Universidad Peruana Cayetano Heredia, 31 Lima, Perú
[15]Instituto de Alta Investigación, Universidad de Tarapacá, Arica 1000000, Chile

(Affiliations continued on next page)

SUMMARY

Dental morphology varies greatly throughout evolution, including in the human lineage, but little is known about the biology of this variation. Here, we use multiomics analyses to examine the genetics of variation in tooth crown dimensions. In a human cohort with mixed continental ancestry, we detected genome-wide significant associations at 18 genome regions. One region includes *EDAR*, a gene known to impact dental features in East Asians. Furthermore, we find that *EDAR* variants increase the mesiodistal diameter of all teeth, following an anterior-posterior gradient of decreasing strength. Among the 17 novel-associated regions, we replicate 7/13 in an independent human cohort and find that 4/12 orthologous regions affect molar size in mice. Two association signals point to compelling candidate genes. One is ~61 kb from *PITX2*, a major determinant of tooth development. Another overlaps *HS3ST3A1*, a paralogous neighbor of *HS3ST3B1*, a tooth enamel knot factor. We document the expression of *Pitx2* and *Hs3st3a1* in enamel knot and dental epithelial cells of developing mouse incisors. Furthermore, associated SNPs in *PITX2* and *HS3ST3A1* overlap enhancers active in these cells, suggesting a role for these SNPs in gene regulation during dental development. In addition, we document that *Pitx2* and *Hs3st3a1*/*Hs3st3b1* knockout mice show alterations in dental morphology. Finally, we find that associated SNPs in *HS3ST3A1* are in a DNA tract introgressed from Neanderthals, consistent with an involvement of *HS3ST3A1* in tooth size variation during human evolution.

INTRODUCTION

Due to their remarkable preservation and extensive morphological variation, teeth have been used extensively in evolutionary studies. Dental features have contributed importantly to taxa definition and phylogenetic analyses, including in hominins.[1] Furthermore, anthropological studies have documented extensive variation in dental morphology within and among modern human populations,[2] dental features being used in applications ranging from population history analyses to individual identification.

Maria-Cátira Bortolini,[13] Giovanni Poletti,[14] Carla Gallo,[14] Francisco Rothhammer,[15] Winston Rojas,[16] Youyi Zheng,[17] James C. Cox,[18] Vaishali Patel,[19] Matthew P. Hoffman,[19] Li Ding,[1] Chenchen Peng,[1] Justin Cotney,[5] Nicolas Navarro,[9,10] Timothy C. Cox,[18,20] Miguel Delgado,[1,21,22,25,*] Kaustubh Adhikari,[23,24,25,28,*] and Andrés Ruiz-Linares[1,3,24,25,29,*]

[16]GENMOL (Genética Molecular), Universidad de Antioquia, 5001000 Medellín, Colombia
[17]State Key Lab of CAD&CG, Zhejiang University, Yuhangtang Road, Hangzhou 310058, China
[18]Department of Oral and Craniofacial Sciences, School of Dentistry, University of Missouri, Kansas City, MO 64108, USA
[19]Matrix and Morphogenesis Section, NIDCR, NIH, DHHS, Bethesda, MD 20892, USA
[20]Department of Pediatrics, School of Medicine, University of Missouri, 400 N Keene St., Kansas City, MO 64108, USA
[21]División Antropología, Facultad de Ciencias Naturales y Museo, Paseo del Bosque s/n, Universidad Nacional de La Plata, La Plata 1900, República Argentina
[22]Consejo Nacional de Investigaciones Científicas y Técnicas, CONICET, Godoy Cruz, 2290 Buenos Aires, República Argentina
[23]School of Mathematics and Statistics, Faculty of Science, Technology, Engineering and Mathematics, The Open University, Walton Hall, Milton Keynes MK7 6AA, UK
[24]Department of Genetics, Evolution and Environment, and UCL Genetics Institute, University College London, Gower Street, London WC1E 6BT, UK
[25]These authors contributed equally
[26]X (formerly Twitter): @Qing_erLi
[27]X (formerly Twitter): @PierreHenriFaux
[28]X (formerly Twitter): @kaustubhad
[29]Lead contact
*Correspondence: medelgado@fcnym.unlp.edu.ar (M.D.), k.adhikari@ucl.ac.uk (K.A.), a.ruizlin@ucl.ac.uk (A.R.-L.)
https://doi.org/10.1016/j.cub.2024.11.027

The use of dental features in evolutionary and anthropological studies is predicated on these features being under strong genetic control. Quantitative genetic analyses in humans have estimated a moderate to high heritability (~50%–90%) for dental crown morphology.[3,4] Furthermore, animal studies have identified dozens of genes involved in dental development (http://bite-it.helsinki.fi), and mutations in some of these genes have been shown to result in rare dental anomalies in humans.[5] However, little is known about the genetic basis of variation in dental morphology in the general population. Candidate gene analyses have reported a few associations with certain dental features.[6,7] Although genome-wide association studies (GWASs) have been reported for some oral traits (e.g., caries, periodontal disease, and age of dental eruption), to our knowledge no such study has been published for tooth morphology. Elucidating the genetic basis of dental variation in the population should help throw light on the evolutionary and developmental processes underlying morphological change.

In recent decades, genome-wide analyses have led to the identification of a plethora of SNPs associated with common phenotypic variation, including certain morphological traits.[8] However, our understanding of the biological basis for these statistical associations is generally incipient. This is usually so because the statistical effects involve non-coding SNPs and occur in linkage disequilibrium blocks, complicating the distinction between "causal" and "non-causal" associations. The biological mechanism underlying causal associations is thought to relate to the involvement of SNPs in regulating the expression of "effector genes" (i.e., those involved in biochemical and cellular pathways relevant to the phenotype studied). Functional genomics technologies are providing powerful tools to examine, at the cellular level, gene expression regulation, thus helping to shed light on the biology of GWAS associations. However, the application of cell-specific omics technologies to dental phenotypes is in its infancy.

Here, we aim to harness genomic and cell-specific functional genomic analyses to explore the genetic basis of variation in human dental morphology. We obtained three dental crown measurements (mesiodistal and buccolingual diameters and height) in a sample of Colombians of mixed European, Native American, and African ancestry. We detected an effect of continental ancestry on dental dimensions and identified significant associations at 18 genome regions. The most robust genome-wide associations were observed in the *EDAR* gene region, with Native American variants increasing the MDD of all teeth following an anterior-posterior gradient. The other 17 genomic associations we detect are novel. We show that most of these associations replicate in a second human cohort, and certain homologous regions also affect molar morphology in mice. Several of the associated regions point to prominent effector genes, particularly *PITX2* and *HS3ST3A1*. We obtained mouse embryo multiomics data showing that associated SNPs in the *PITX2* and *HS3ST3A1* regions overlap enhancers active in key cell types during dental development. We further show that mice deficient for *Pitx2* and *Hs3st3a1* present alterations of crown morphology, supporting their conserved function in influencing tooth form. Finally, we find that associated SNPs in *HS3ST3A1* are in a DNA tract introgressed from Neanderthals, pointing to an involvement of this gene in human tooth size evolution.

RESULTS

Study sample and data examined

We obtained 3D surface scans of dental plaster casts from 882 Colombian volunteers and used automatic segmentation procedures to isolate and orientate incisors (I1 and I2), canines (C), premolars (P1 and P2), and molars (M1 and M2) (Figure 1). We then measured the mesiodistal and buccolingual crown diameters (henceforth MDDs and BLDs) and clinical crown height (henceforth height/H; see STAR Methods) of each available tooth (Figure 1), resulting in up to 84 measurements being obtained per individual. Intraclass correlation analysis of automatic and manual measurements, obtained in 25 individuals, indicated a good reliability of the automatic measurements (Table S1). After

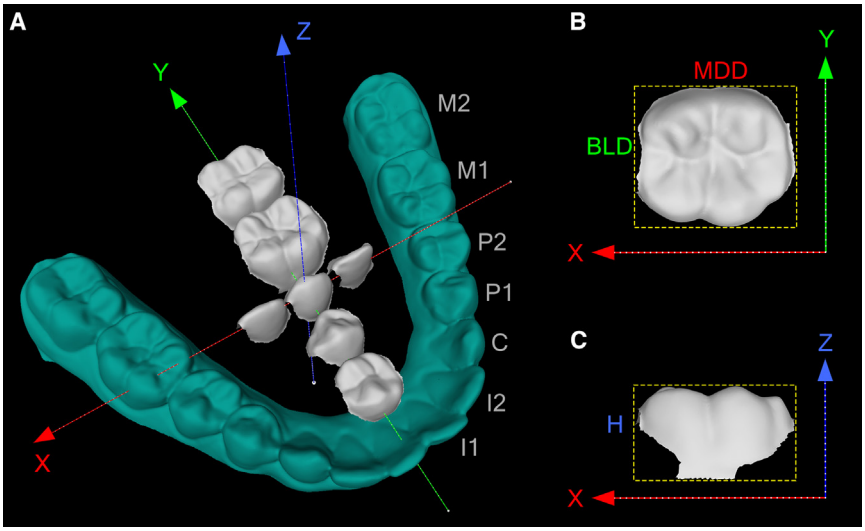

Figure 1. Procedure for 3D phenotypic data collection

Dental crown measurements were obtained for each tooth, after segmentation of a 3D image from a full dental arcade. In (A) are shown example 3D images of a dental cast and segmented teeth. In turquoise is shown the unsegmented dental arcade, with different tooth classes identified (I, incisors; C, canines; P, premolars; M, molars). Within the arcade are shown (in white) examples of individual teeth, obtained after segmentation of the dental arcade. The segmented teeth are aligned along standardized 3D coordinates, from which the mesiodistal diameter (MDD, y axis), buccolingual diameter (BLD, x axis), and height (H, z axis) measurements are obtained. For illustration, example teeth have been slided along the x or y axis. In (B) and (C), we show the planes from which MDD, BLD, and H measurements are obtained for each tooth.

exclusion of outliers (due to occasional segmentation problems), the measurements are approximately normally distributed (Data S1). We performed genome-wide genotyping of the volunteers on Illumina HumanOmniExpress or GSA chips. The resulting data were merged and imputed (using 1000 Genomes Phase III [1000GP3]) up to a total of ~10.3 million SNPs. Based on the chip data, the average genome ancestry for the individuals examined was estimated as ~59% European, ~30% Native American, and ~11% African.

Correlations of dental measurements

We examined correlations between measurements for upper (U) and lower (L) teeth, on both the left (L) and right (R) sides of the dental arcades (Figure S1; Table S2). Strongest correlations ($r > 0.7$) were observed for the same measurements (BLD, MDD, or H) taken on the same tooth (either L/R or U/L) and for comparisons involving teeth of the same class (incisors, premolars, and molars). Stronger correlations were seen for teeth on the same dental arcade than between the upper and lower arcades. Strong correlations between teeth of different classes were seen only for H, possibly due to the sensitivity of this measurement to the extent of exposed tooth root.

We used partial correlations to examine the effect on left/right averaged BLD, MDD, and H of age, sex, stature, and continental genetic ancestry (considering upper and lower dentition separately, Table S3). Moderate (significant) correlations were observed for age with H for all teeth ($0.12 < r < 0.34$), probably reflecting increased tooth root exposure with age. Low/moderate (significant) correlations with sex were observed for most crown measurements ($0.01 < r < 0.28$), males having larger teeth than females, the largest sexual dimorphism being observed for canine dimensions, in agreement with previous studies (Table S3; Figure S2).[9] Non-significant correlations were observed between dental dimensions and stature, with the exception of BLD, which for certain teeth showed a low (<0.16) but significant correlation. Low/moderate (significant) correlations ($0.07 < r < 0.28$) were observed for genetic ancestry with dental crown dimensions: the strongest effects were seen for MDD and BLD of premolars, with African and Native American ancestry increasing these dimensions, relative to European ancestry (Table S3). This observation agrees with anthropological surveys reporting that Europeans have the smallest crown BLD and MDD among continental populations.[10]

Overview of GWAS results

Initial analyses examined SNP association with left/right average MDD, BLD, and H measurements for each tooth (a total of 42 traits). We observed genome-wide significant association (p value $< 5 \times 10^{-8}$) in eight genome regions, involving 439 SNPs and 13 traits (Figure 2; Table S4). Three regions were associated with MDD, three with H, and two with BLD. One region (on 2q12) was significantly associated with the MDD of six different teeth and showed suggestive association (p value $< 10^{-5}$) for the MDD of three other teeth, always resulting in an increased MDD (for the remaining five teeth, the effects were in the same direction, but association p values were below significance). Two regions (on 8p23.2 and 16q24.1) significantly associated with LI2 H and UC BLD, respectively, were also suggestively associated with the same measurement in other teeth (always involving the same dimension: H or BLD, Figure 2; Table S5). The other significant associations involved a single tooth. When comparing the upper and lower dental arcades for the eight significantly associated regions, more associations were detected in the upper (8 significant, 4 suggestive) than in lower arcade (5 significant, 2 suggestive).

Since we found strong correlations between measurements for teeth of the same class (Figure S1), we also performed a multivariate analysis (Wald test) grouping measurements obtained in incisors, canines, premolars, or molars (but analyzing separately upper and lower dentition, resulting in 24 traits being examined). A total of 11 genome regions showed significant associations (p value $< 5 \times 10^{-8}$, involving 114 SNPs and 10 measurements; Figure 2; Table S4). Among these 11 regions, 6 were associated with MDD, 3 with BLD, and 2 with H. As seen in the univariate analyses, 2q12 shows significant effects on MDD for the upper and lower dentition. Incisor MDD is significantly associated with four genome regions (Figure 2; Table S4). All other traits were associated with a single genome region. All

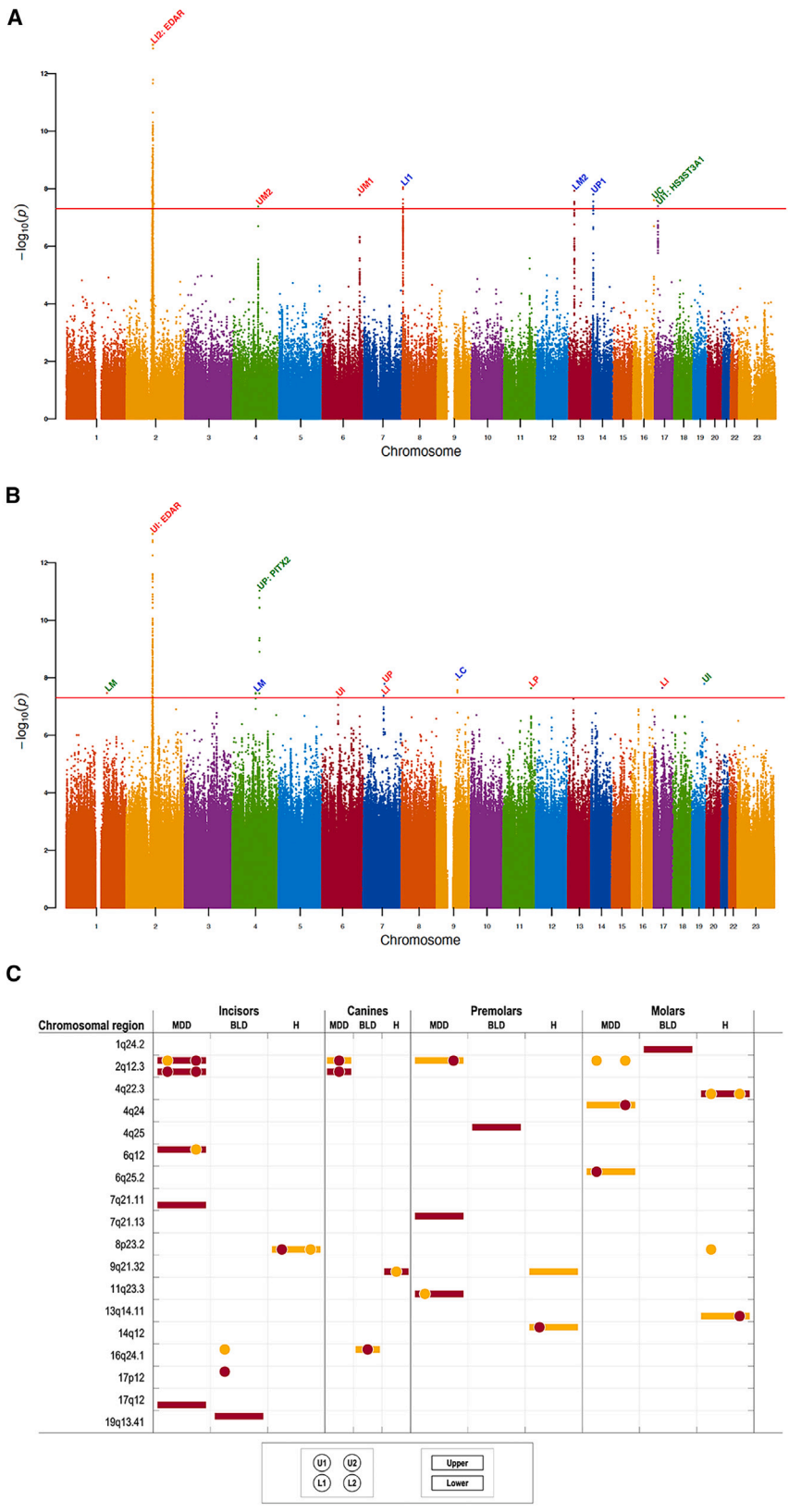

Figure 2. Summary of GWAS results

(A) Manhattan plot displaying the location of regions significantly associated with at least one (left-right average) measurement, i.e., the BLD, MDD, or H obtained on each of the upper (U) and lower (L) incisors (I1 and I2), canines (C), premolars (P1 and P2), and molars (M1 and M2). The genome-wide significance threshold is indicated by a red line ($<5 \times 10^{-8}$). For each significant hit, the tooth in which the strongest association was detected is shown (color indicating the measurement involved: green: BLD, red: MDD, blue: H). The location of *EDAR* and *HS3ST3A1* in the 2q12 and 17p12 regions, respectively, is indicated.

(B) Manhattan plot displaying the location of significant hits based on a Wald test applied to the BLD, MDD, and H measurements for teeth of the same class, i.e., incisors (I), canines (C), premolars (P), and molars (M), from the upper/lower dental arcades. The location of *EDAR* and *PITX2* in the 2q12 and 4q25 regions, respectively, is indicated.

(C) Summary of association results, across all measurements, for the index SNPs in the 18 regions with at least one genome-wide significant association. Colored dots/bars at the top/bottom of each cell refer to results from teeth in the upper/lower arcade. Left/right position of dots on the cell refers to the first/second tooth for each class. Bars refer to results from a Wald test combining measurements for teeth of the same class. Genome-wide significant p values ($<5 \times 10^{-8}$) are indicated in red, and suggestive p values (between 5×10^{-8} and 10^{-5}) are in yellow.

See also Tables S4 and S5 and Data S2.

Table 1. Follow-up of novel GWAS hits in a Chilean replication sample and in a mouse QTL analysis

Region[a]	Index SNP	*p* value	Replication SNP	Replication *p* value[b]	Mouse QTL *p* value[c]
1q24.2	*rs9332575*	*3.37E−8*	N/A	N/A	4.52E−6[d]
2q12.3	rs3827760	7.55E−20	rs3827760	7.27E−5[d]	N/A
4q22.3	*rs62306712*	*3.39E−8*	rs6840219	4.36E−3[d]	N/A
4q24	rs9995250	4.11E−8	rs9995250	1.40E−1	N/A
4q25	*rs3866831*	*9.45E−12*	rs3866831	5.10E−2	1.56E−5[d]
6q12	*rs4710320*	*4.96E−8*	N/A	N/A	N/A
6q25.2	rs71803342	1.65E−8	rs71803342	5.56E−2	7.09E−4
7q21.11	*rs374151389*	*4.27E−8*	rs374151389	7.35E−3	N/A
7q21.13	*rs200603184*	*1.63E−8*	N/A	N/A	N/A
8p23.2	rs202037377	8.74E−9	rs202037377	1.74E−3[d]	1.01E−3
9q21.32	*rs7870024*	*1.17E−8*	rs7870024	5.47E−2	6.54E−3
11q23.3	*rs34750993*	*2.32E−8*	rs34750993	1.76E−3[d]	N/A
13q14.11	rs9562329	1.20E−8	rs9566820	1.54E−2[d]	2.78E−4
14q12	rs3940231	1.57E−8	rs3940231	1.13E−2[d]	N/A[d]
16q24.1	rs11646373	2.53E−8	rs11646373	1.30E−1	7.40E−4
17p12	rs35674068	3.98E−8	rs35865369	1.25E−3[d]	1.71E−5[d]
17q12	*rs8076153*	*2.27E−8*	rs8076153	1.59E−2[d]	2.42E−5[d]
19q13.41	*rs7251705*	*1.64E−8*	N/A	N/A	N/A

See also Tables S4 and S7.

[a]Regions detected in the Wald test are in italics (the 2q12.3 region was also significant in the regular GWAS).

[b]Replication *p* values from single-trait associations had an FDR-adjusted significance threshold of 0.0154; the significance threshold for the Wald test associations is 0.0324. Significant values are shown in bold. N/A indicates the SNP was not available for testing in the replication cohort.

[c]The FDR-adjusted significance threshold is 10^{-4}, corresponding to an FDR < 5%. N/A indicates the homologous region was not reliably mapped in mice.

[d]Significant values.

significant regions detected in the univariate analyses produced suggestive associations in the multivariate GWAS, with the 2q12 association with MDD being significant in both univariate and multivariate tests (Table S5). Conversely, several of the regions significant in the Wald test were suggestively associated in the univariate tests (Table S5). The partial overlap between the uni- and multivariate analyses is consistent with the varying statistical power of these two types of tests to detect tooth-specific effects versus pleiotropic effects involving teeth with correlated measurements.

Follow-up of GWAS hits

For replication analyses of the 17 novel hits detected here, we examined an independent sample of 186 individuals (33% males and 67% females), aged 18–45 years (mean = 33), recruited in Arica, Chile. Processing of phenotypic and genotypic data in this sample was as in the Colombian sample, with average ancestry in the Chileans estimated as 3.4% African, 51.5% European, and 45.1% Native American. We focused on replication of the index SNPs at the associated regions detected in the GWAS, using the same tests as in the Colombian sample. When the index SNP was unavailable in the Chilean sample, we tested a proxy SNP (in LD with the index SNP and associated at least at a suggestive threshold in the Colombian GWAS). Overall, 13/17 of the novel regions could be tested in the Chilean sample, and 7/13 were significantly associated with dental crown measurements, after a false discovery rate (FDR) multiple-testing correction (Table 1).

We also evaluated if SNPs in mouse genome regions homologous to the newly associated regions detected in the GWAS impact on molar size in outbred mice. We examined publicly available data from Facebase, comprising micro computed tomography (microCT) skull scans and data for ~60,000 SNPs genome wide.[11,12] We obtained MDD and BLD measurements from the three upper and lower molars in ~1,000 mice. Since soft tissue was not reliably recoverable with the scan parameters used by FaceBase, H was not obtained from the mouse scans. Therefore, we only tested in mice the 12 regions associated with MDD or BLD in humans. A quantitative trait locus (QTL) analysis indicates that four of these regions (homologous to human 1q24.2, 4q25, 17p12, and 17q12) have significant effects on mouse molar MDD or BLD (Table 1).

A gradient for the effect of *EDAR* on tooth crown MDD

In the univariate analyses, we observed that the *EDAR* region is significantly associated with the MDD of 6 teeth: first lower incisor, second lower incisor, second upper incisor, lower canine, upper canine, and second upper premolar (Figure 2; Table S5). *EDAR* is also suggestively associated with MDD of the first upper incisor, first and second upper molars (Figure 2; Table S5). The strongest association is seen for incisors and the weakest for molars. Comparing the effect size divided by MDD across tooth classes, we observe an anterior-posterior gradient for the effect of *EDAR* on MDD (Table 2): incisors show the largest effect (0.028) followed by canines (0.019), with premolars and molars having the smallest effects (0.015

Table 2. Effect of *EDAR* on the MDD of different teeth

	UI1	UI2	LI1	LI2	UC	LC	UP1	UP2	LP1	LP2	UM1	UM2	LM1	LM2
Effect (beta/MDD)[a]	0.018	0.038	0.027	0.031	0.017	0.022	0.016	0.022	0.008	0.014	0.014	0.017	0.013	0.006
Average effect		0.028			0.019			0.015				0.012		
Wald test *p* value[b]		<1E−16			1.37E−8			3.68E−4				1.26E−4		

[a]To enable comparison across different tooth classes, the effect estimated from the regression analysis (beta) was divided by the MDD. All values shown are for index SNP (rs3827760).
[b]The Wald test was applied to each class of teeth (incisors, canines, premolars, and molars), using measurements for left, right, upper, and lower teeth.

and 0.012, respectively). A similar trend is observed comparing the *p* values from the Wald test across tooth classes (Table 2).

Cell-type-specific enhancer activity and candidate gene expression

Several of the associated regions point to candidate effector genes with independent evidence for an involvement in dental development. The *EDAR* region is the only case for which various studies suggest that the phenotypic association relates to the impact of an amino-acid substitution on EDAR activity during development. In the novel regions detected here, all but one of the associated SNPs are non-coding and located in intronic or inter-genic regions. This agrees with evidence indicating that SNPs associated with human morphological variation mostly mediate their effects through regulatory effects on nearby developmental genes.[13–15] To evaluate the relationship of associated SNPs with enhancer activity and gene expression during dental development, we obtained single-nucleus multiome (single nucleus RNA sequencing [snRNA-seq] and single nucleus assay for transposase-accessible chromatin sequencing [snATAC-seq]) data from cap stage mandibular incisors at embryonic day 13.5 (E13.5). We identified 11 cell-specific gene expression signatures. From these, we identified active enhancers and predicted enhancer:gene interactions in associated regions at cell-type resolution (Figure S3). Below we highlight results for the most prominent candidate genes potentially mediating the phenotypic associations for two genome regions (in Data S2, we present results for other associated regions).

4q25: PITX2

SNPs in 4q25 showed significant association with the BLD of upper premolars (UP) in the Wald test (Figure 3A strongest *p* value of 9.45×10^{-12} for rs3866831). Significant association of SNPs in this region with BLD of maxillary and mandibular third molars was also observed in outbred mouse data (Table 1). The closest gene to the association peak (~60 kb upstream) is the paired like homeodomain 2 (*PITX2*) gene. Experimental studies have shown that *Pitx2* plays a prominent role in mouse development, including teeth.[16] As expected from previous studies, we find that E13.5 multiome data show expression of *Pitx2* in dental epithelium, including enamel knot cells (*Pitx2* having been established as one of the expression markers for this cell type; Figure 3C). The associated region identified here (BP: 111,624,540–111,732,114) is in LD with enhancer elements active in enamel knot and dental epithelium cells (Figure 3B). A recent GWAS of facial features reported an association of SNPs in 4q25 with maxillary morphology.[15] The index SNP associated with facial shape in 4q25 is 14 kb from the index SNP identified here (rs3866831; $r^2 = 0.4$), suggesting that variants in this genome region could impact patterning and scaling in multiple orofacial contexts.

17p12: HS3ST3A1

The SNPs in 17p12 associated with BLD of upper central incisors (UI1) overlap heparan sulfate-glucosamine 3-sulfotransferase 3A1 (*HS3ST3A1*) (Figure 3D) and are all non-coding. Significant association for the index SNPs in this region with dental dimensions was also observed in the Chilean replication sample, and, in mice, SNPs in the homologous region are associated with molar dimensions (Table 1). There is no previous evidence for the involvement of *HS3ST3A1* in dental development. However, a paralogous gene ~800 kb from *HS3ST3A1* encodes HS3ST3B1 (Figure 3D), which has recently been identified as a novel enamel knot factor.[17] It has long been known that the enamel knot determines the size, shape, and cusp morphology of developing teeth.[18] The cell-type-specific multiome data we obtained shows expression of *HS3ST3A1* in bone progenitor, dental mesenchyme, and enamel knot cells at E13.5 (Figure 3F). Furthermore, the associated 17p12 SNPs (genome coordinates: 13,402,978–13,453,558) overlap enhancer elements active in all these same cell types, with certain enhancers predicted to regulate expression of *HS3ST3A1* (Figure 3E). These regions are also predicted to physically contact regulatory regions alongside *HS3ST3B1*, suggesting a potential coregulation of these two genes.

Dental morphology in *Pitx2* heterozygote and *Hs3st3a1;Hs3st3b1* mutant mice

Homozygous null *Pitx2* mice, which die at birth due to cardiac anomalies, have previously been reported to have hypoplastic maxillary and mandibular prominences with tooth development arrested at the bud stage.[19] Therefore, to evaluate the potential effect of *Pitx2* expression on mouse tooth size, we examined molar size in heterozygous *Pitx2* mutant mice following 3D rendering of reconstructed microCT scans. Upon visual inspection, all control mice presented with the expected number (three), morphology (overall and cusp number), and size of molars in the maxillae and mandibles. In contrast, we noted one *Pitx2* heterozygote was missing a right maxillary third molar and had a small additional molar anterior to the first molar on the left hemimandible. Furthermore, compared with controls, all remaining *Pitx2* heterozygotes presented bilaterally with visibly small maxillary and mandibular third molars, with the maxillary third molars appearing smaller than the mandibular third molars. In addition, all mandibular second molars in *Pitx2* heterozygotes and the second maxillary molars in two of these mice were also missing a cusp (Figure 4).

Consistent with the previously reported association of *PITX2* SNPs with maxillary morphology,[15] measurements of the maxillary and mandibular alveolar lengths revealed *Pitx2* heterozygotes

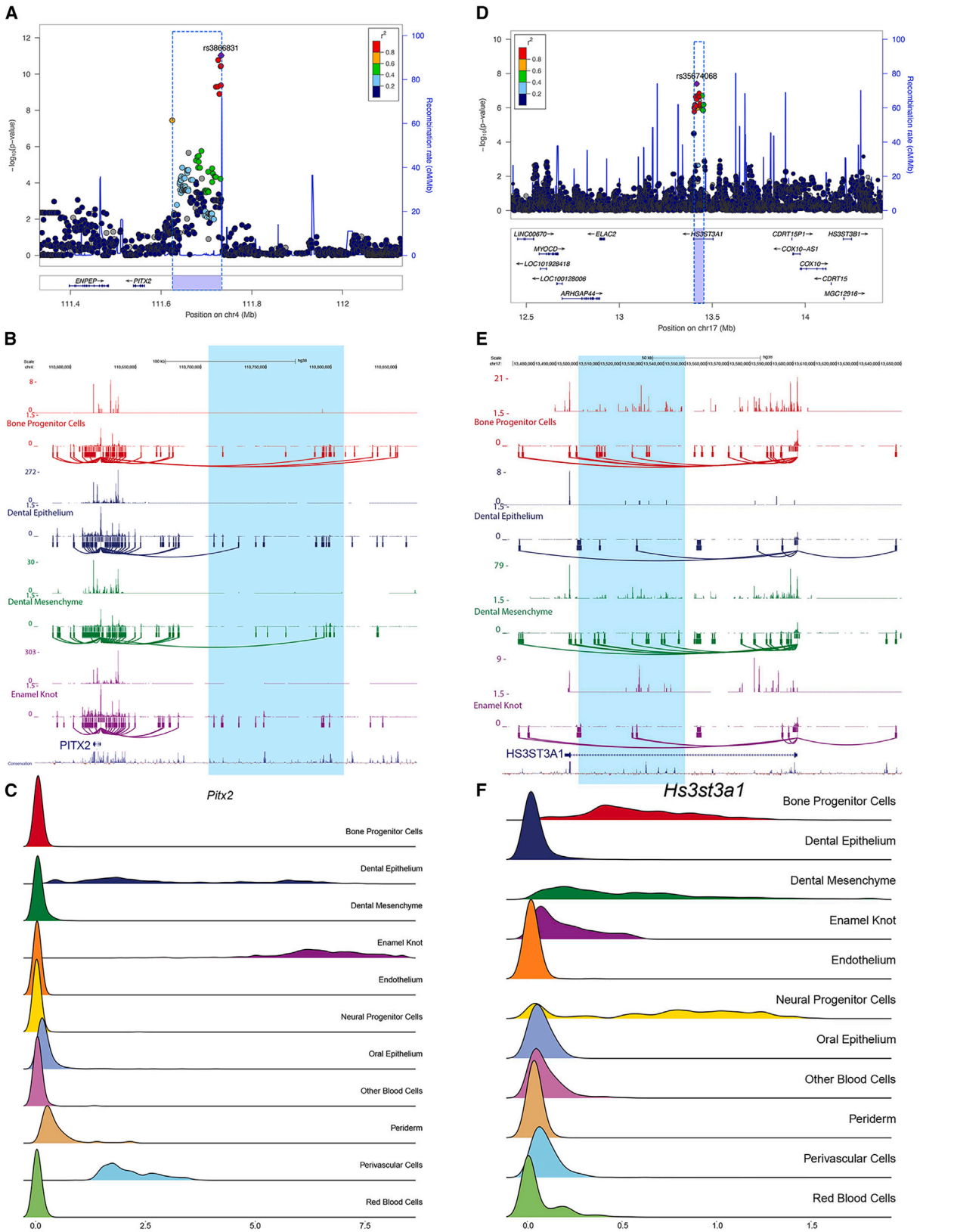

(legend on next page)

to be ~4.3% (p value = 2.15 × 10^{-3}) and 3.6% (p value = 4.43 × 10^{-5}) shorter, respectively, than wild-type littermate controls, regardless of sex. The maxillary molar tooth row lengths (sum of MDDs of the three molars) were ~6.1% shorter than controls (p value = 6.98 × 10^{-5}), while mandibular molar tooth row lengths were ~2.5% (p value = 3.91 × 10^{-2}) shorter than controls. However, when considering the ratio of average alveolar length to average total molar row length, only the maxillary ratio was significantly different between heterozygotes and controls (p value = 0.036), indicating that the maxillary molar row was disproportionately smaller in *Pitx2* heterozygotes. Assessment of the MDD and BLD of individual maxillary molars confirmed the small third molars but also highlighted smaller MDD and BLD for the first maxillary molars in heterozygotes compared with controls.

A similar evaluation of crown morphology was undertaken for *Hs3st3a1; Hs3st3b1* double knockout (DKO) mice. Qualitative assessment of *Hs3st3a1; Hs3st3b1* and age, sex, and genetic background-matched controls also revealed small maxillary third molars in all DKO mice, with additional morphological anomalies seen in some teeth. These included cusp size, number, and shape anomalies affecting all three maxillary molars (Figure 4). No overt defects in morphology were observed in the mandibular molars. Quantitative analysis showed a significantly reduced MDD of the maxillary third molar (p value = 1.30 × 10^{-7}) but not of BLD (p value = 0.90). Overall, the total maxillary molar row length was not significantly different between mutants and controls (p value = 0.14), although the total molar row length showed marked variability. In addition, the maxillary first molar of the DKO mice was found to be larger in both BLD (p value = 1.53 × 10^{-2}) and MDD (p value = 3.01 × 10^{-2}) compared with age- and sex-matched controls (Figure 4). Notably, BLD of the maxillary incisors was also shown to be decreased (p value = 1.41 × 10^{-2}) for the DKO mice, but MDD was not significantly different from controls (p value = 0.16). Furthermore, in *Hs3st3a1;Hs3st3b1* DKO mice, the mandibular alveolar length (1.69 × 10^{-2}), but not the maxillary alveolar length (p value = 0.15), was significantly shorter than controls. In contrast to the *Pitx2* heterozygous mice, only the mandibular average alveolar length to total molar row length ratio was significantly different between DKO mice and controls (p value = 1.84 × 10^{-4}). Notably, the BLD:MDD ratio—a measure of overall crown size—showed significantly increased variation in dimensions of all teeth in the DKO mice compared with controls (Levene's test: M1: p = 0.017; M2: p = 0.043; M3: p = 0.000046; I: p = 0.039; see Figure 4E).

Neanderthal introgression in associated regions

We screened for Neanderthal introgression at the 18 genome regions associated here with dental measurements. We focused on detecting introgression tracts in a 1 Mb window centered around the index SNP of each region. Considering only introgression tracts called with >99% confidence, >25 kb in size, and with a frequency >1% in the Colombian sample, we detected Neanderthal introgression in 14/18 regions. Using an admixture mapping approach, we defined 261 Neanderthal segments in these regions and tested for association of each segment with the phenotypes examined in the Colombian sample. We found that Neanderthal introgression segments in the 17p12/*HS3ST3A1* region are significantly associated with BLD of UI1 (p value = 2.4 × 10^{-7}; Figure 5), consistent with the effect seen for SNPs in this region in the GWAS analyses. The Neanderthal segment with the strongest association spans ~20 kb and includes the GWAS index SNP in this region (rs35674068). The introgression signal we detected in 17p12 overlaps a similar signal reported in a previous analysis of 379 Europeans and 286 East Asians.[20] This signal was also detected with an alternative method in our data (IBDmix[21]—Figure S4). Contrasting introgression calls in 17p12 with calls of local ancestry (African, European, or Native American ancestry), we infer that Neanderthal introgression in this region is contributed by the European ancestry component in the Colombian sample (Figure S5; Table S4).

DISCUSSION

The number, size, and shape of teeth varies greatly throughout the evolution of vertebrates, including mammals.[22] This variation has generally been thought to reflect evolutionary adaptation, particularly to changes in diet.[23] Consistent with the macroevolutionary role of adaptation during tooth morphology evolution, signals of positive selection have been reported in mammals at certain genes expressed during dental development.[24,25] In hominins, a reduction in tooth size has been documented from the middle Pleistocene to the present, this reduction being observed also in prehistoric modern humans across the world over the last several millennia.[26] Several explanations have been proposed for this reduction in hominin tooth size, particularly the change to a softer diet resulting from new food preparation and processing techniques.[27] Modern human populations across the world also show variation in various metric and nonmetric dental features.[10] In contrast to long-term evolutionary trends, it has been argued that variation in dental morphology among contemporary human populations does not result from adaptation but could mostly be neutral.[2] Furthering our understanding of the genetics basis of dental variation should help throw light on the evolutionary forces shaping tooth morphology and its developmental basis.

The effects we detect of continental genetic ancestry on BLD and MDD agree with anthropological studies documenting smaller crown sizes in Europeans, relative to Africans and Native Americans.[10] The dental morphology differentiation between continental populations and the effect of genetic ancestry on

Figure 3. Regional association, cell-type-specific predicted enhancer: gene connections and gene expression in 4q25 and 17p12

Regional association, cell-type-specific predicted enhancer: gene connections and gene expression in 4q25 (A–C) and 17p12 (D–F). (A and D) SNP association p values (colors reflecting LD with the labeled index SNP). The positions of the *PITX2* gene (A) and *HS3ST3A1* and *HS3ST3B1* genes (D) are shown underneath. (B and E) Cell-type-specific chromatin profiling in developing mouse incisor buds. For each cell type, the top row shows ATAC-seq, the second row shows peak calls from ATAC-seq, the third row shows enhancers called from ATAC peaks, and the fourth row shows predicted enhancer:gene connections. Shaded in blue in (A), (D), (B), and (E) is the region comprising SNPs associated at genome-wide significance. (C and F) Expression plots for *Pitx2* (C) and *Hs3st3a* (F) in developing mouse incisor bud cells (x axis is gene expression, in transcripts per million, and y axis is the number of cells from that cluster).

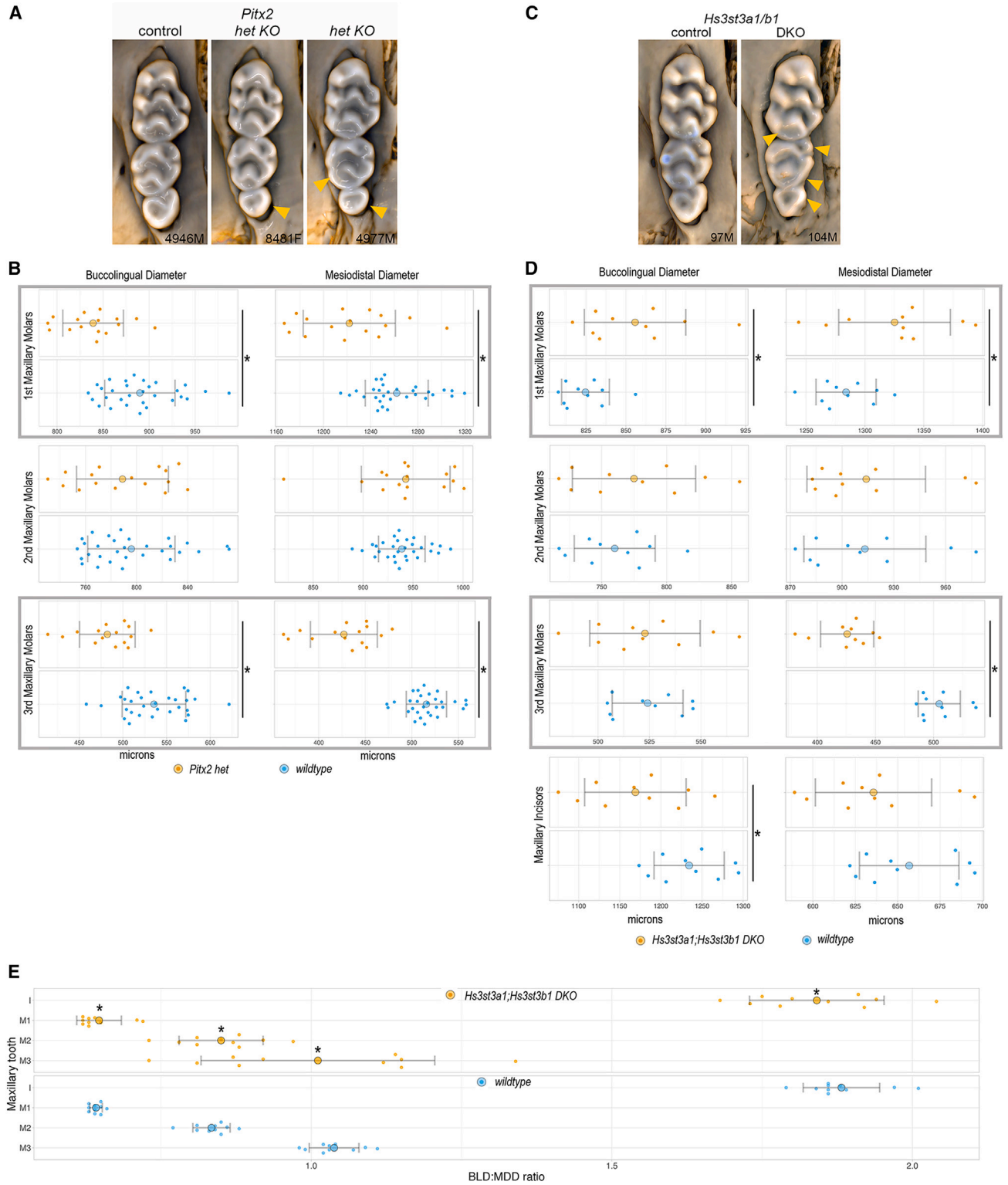

Figure 4. Crown size differences in *Pitx2* heterozygous KO mice and *Hs3st3a1;Hs3st3b1* DKO mice

(A) Examples of maxillary molar rows from control (wild-type) and *Pitx2* KO heterozygotes. The small third molar and second molar cusp anomalies are marked (yellow arrowheads).

(B) Buccolingual diameter (BLD) and mesiodistal diameter (MDD) of individual maxillary molars in control and *Pitx2* heterozygotes. Error bars represent the standard deviation of the measurements.

(legend continued on next page)

BLD and MDD detected here are consistent with the existence of allelic variants impacting crown dimensions with differentiated frequencies between continental populations. A prominent example is SNPs in the *EDAR* region, where associated alleles are seen at high frequency only in East Asians and Native Americans (Tables 1, 2, and S4). Consistent with the effect of genomic ancestry, we find that the Native American alleles in *EDAR* increase MDD for all teeth. These *EDAR* alleles are in strong LD over a large genome region (of ~2 Mb), which appears to have been under strong recent selection,[28,29] and includes a V370A gain-of-function substitution in EDAR (rs3827760).[28] Early candidate-gene studies associated this V370A variant with hair thickness and shovel-shaped incisors (SSIs) in East Asians.[6] Furthermore, recent GWASs have demonstrated a high pleiotropy for *EDAR* SNPs, associating these with a range of tegumentary and facial features.[13,14,30–32]

The anterior-posterior effect gradient we observe for *EDAR* SNPs on tooth MDD agrees with studies in East Asians showing a stronger association of rs3827760 with crown size for anterior (incisors and canines) than for posterior (premolars and molars) teeth.[6] Furthermore, a positive correlation has been reported between MDD and SSI in East Asians, possibly reflecting enamel overgrowth.[6] Consistent with the stronger effect of *EDAR* on anterior teeth, rare mutations involving *EDAR* have been shown to lead to selective tooth agenesis, preferentially involving anterior teeth.[33] Furthermore, *EDAR* mouse mutants show a complete loss of enamel in incisors but only reduced enamel in molars.[34] These observations agree with teeth developing in an antero-posterior direction[1] and the proposal that "pattern genes" affect tooth development following a modular framework, coinciding with the proposed Turing-type mechanism of activation of signaling centers that establish repeated patterns during morphogenesis.[35] This is supported by studies in mice showing a developmental role for Eda/Edar signaling in anterior-posterior patterning of the incisor and molar tooth buds[36] and its key role in driving the evolutionary trajectories of specific dental morphologies.[37] Although here we detect significant pleiotropic effects only for *EDAR*, pleiotropy is probably present for other loci, but detecting such effects through statistical association will require additional population studies.

It is possible that the strong phenotypic effect of *EDAR* on dental and other tegumentary phenotypes relates to the functional impact of the V370A EDAR substitution. By contrast, multiomics studies have shown that SNPs associated with facial morphology and with tooth eruption/number of teeth are overwhelmingly non-coding and enriched in gene expression regulatory elements active during craniofacial development.[13,14] Consistently, in the novel regions we detected here, we find only one other missense SNP associated at genome-wide significance (in the *RABGGTA* gene in 14q12; Data S2). Furthermore, our RNA-seq analyses confirm that SNPs associated with dental dimensions overlap enhancers active during dental development in key cell types (Figure 3; Table S4). In addition, the KO mouse mutants we examined directly confirm a conserved evolutionary role for expression levels of *PITX2* and *HS3ST3A1-HS3ST3B1* influencing normal dental dimensions and morphology (Figure 4). Interestingly, the overlap of *HS3ST3A1* alleles associated with a reduction in UI1 BLD with a signal of Neanderthal introgression (Figures 3 and 5) suggests that *HS3ST3A1* regulation could have also played a role in tooth size reduction both in archaic and modern humans. Of relevance, trends for reduction in tooth size, enamel thickness, and coronal dentine have been reported in hominins, from the Plio-Pleistocene onward.[27] Furthermore, *HS3ST3A1* Neanderthal alleles are common in Europeans but have low frequencies in Africans and East Asians (Table S4), suggesting that these alleles could contribute to the differentiation of dental size between Europeans and non-Europeans.[10]

PITX2, a member of the highly conserved PITX homeobox transcription factor family, plays a critical role in pituitary, facial, dental, cardiac, intestinal, and muscle development.[38] The involvement of *PITX2* in tooth morphogenesis is well established, with this gene being expressed in the dental epithelium from the earliest developmental stages and throughout tooth morphogenesis.[39] Mutations in *PITX2* cause Rieger syndrome type 1, an autosomal dominant disorder whose cardinal features include hypodontia (and other dental abnormalities), often affecting maxillary premolars,[40] and a flattened midface. *Pitx2*-null mutant mouse embryos have arrested tooth development at placode or bud stage. Heterozygote mutants have been previously described as normal,[16] but here, we show that these mutants in fact have reduced dimensions of the first and third molars, as well as various molar cusp shape deviations, and mildly shortened maxillae.

HS3ST3A1 and HS3ST3B1 are enzymes synthesizing 3-O-sulfated heparan sulfate (HS) moieties. These genes are widely expressed, with HS impacting the activity of a wide range of membrane receptors and ligands, including fibroblast growth factors (FGFs) and their receptors. It is well established that FGFs play an important role in tooth development, repair, and regeneration,[41] including interactions with PITX2. Both *Hs3st3a1* and *Hs3st3b1* are expressed in fetal submandibular gland end bud and myoepithelial cells, both of which are progenitor cells during development and regeneration.[42] *Hs3st3b1* has been recently identified as a novel enamel knot factor with a high likelihood of involvement in human non-syndromic dental phenotypes.[17] The enamel knot has long been known to influence tooth size and shape. Our analysis of tooth dimensions, both in outbred mouse crosses and in *Hs3st3a1;Hs3st3b1* DKO mice, and enhancer contacts in dental cell populations, supports direct roles for both of these genes in dental crown morphology.

We hypothesize that the sensitivity of the first and third molars, but not the second molars, in both the *Pitx2* KO and

(C) Examples of maxillary molar rows from control (wild-type) and *Hs3st3a1;Hs3st3b1* double knockout (DKO) mice. The small third molar and abnormal molar cusps in the first and second molars seen in mutant mice are marked (yellow arrowheads).
(D) BLD and MDD diameters of individual maxillary molars and incisors in control and *Hs3st3a1;Hs3st3b1* DKO mice. Error bars represent the standard deviation of the measurements.
(E) Comparison of BLD:MDD ratios of each maxillary tooth from control and *Hs3st3a1;Hs3st3b1* DKO mice reveals increased variability of all crown dimensions. Asterisks mark significant differences ($p < 0.05$). Error bars represent the standard deviation of the measurements.
See also Figure S7.

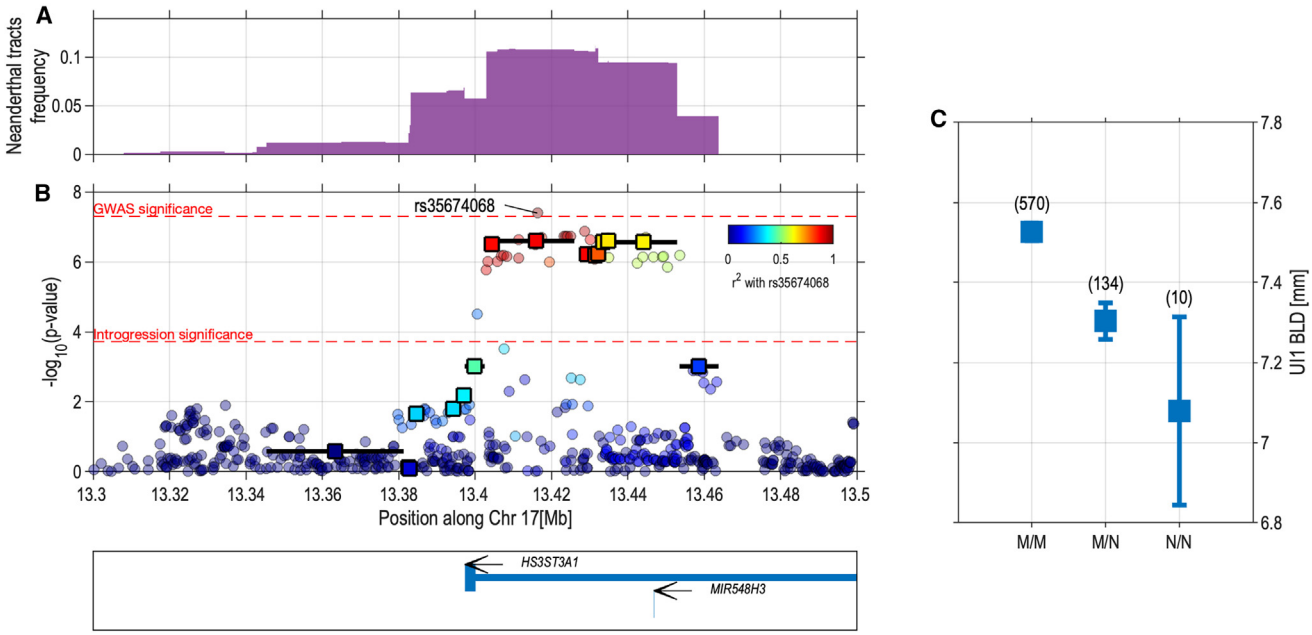

Figure 5. Neanderthal introgression in 17p12 and BLD of first upper incisors (UI1)

(A) Frequency of Neanderthal introgression in the region (Neanderthal tracts called have been aggregated across individuals).

(B) Association −log *p* values for Neanderthal ancestry with UI1 BLD. The squares in the foreground mark the center of a Neanderthal segment with whiskers marking its extent. For reference, SNP association −log *p* values from the GWAS are shown as circles in the background. Colors of squares and circles reflect LD with the index SNP from the GWAS (rs35674068). Gene annotations in the region are shown underneath.

(C) Average UI1 BLD for individuals with different genotypes for the Neanderthal segment showing the strongest association (overlapping the index SNP rs35674068 in B). M, modern human; N, Neanderthal. Vertical bars indicate standard errors, with number of individuals for each genotype in parenthesis.

See also Figure S5.

Hs3st3a1;Hs3st3b1 DKO mice arise through distinct mechanisms. In mice, as in humans, molars develop in an anterior to posterior direction, governed by repeated initiation of signaling centers and gene expression that define the dental placodes and tooth growth. Like other repeated structures in the animal, this is thought to arise through a Turing-type mechanism of sequential patterning.[36] For example, although mice, like other rodents, are characterized by a large diastema between the incisors and molars that is devoid of teeth, they still initiate the early molecular signature of dental placodes in this region. Specifically, two signaling centers and subsequently early tooth buds, defined by activated and spatially restricted gene expression, still form within the diastema segment. However, these recede as the placodes for the eventual first molars form. It is thought that these receding buds can be promoted to continue to form "pre-molars" following disruptions to genes important for this repeated patterning. Such a "pre-molar" was activated in one of the *Pitx2* KO mice in this study, consistent with this gene being a critical early placodal gene. Likewise, the function of Hs3st3a1 and Hs3st3b1 has been proposed to impact signaling of key pathways such as Fgfs, which are known to play an important role in dental placode development. For this reason, the anterior molars are proposed to be more sensitive to perturbation of gene expression, whether through genetic variation or the influence of environmental factors. In contrast, the third molars—both in the maxillae and mandible—are the last to form and erupt. Changes in third molar morphology are common in both humans and mice, with impacts on morphology and eruption sensitive to a multitude of genetic and environmental disruptions.[43] Importantly, third molar size and presence can also be impacted by facial and jaw size.[44] In this regard, in each mutant (*Pitx2* and *Hs3st3a1-b1*), the maxillary and mandibular alveolar bone is shorter than littermate controls. We therefore posit that the altered third molar morphology in these mice could be related to shared or independent mechanisms of these genes in regulating jaw size.

The application of omics technologies to the analysis of tooth morphology is in its infancy. Our results illustrate the potential of this approach to further our understanding of the genetic and cellular basis of dental variation. Additional analyses should shed further light on the developmental processes shaping dental morphology and help clarify debates concerning the forces at play during human dental evolution. A greater understanding of the processes underlying dental morphology variation could also contribute to the development of novel strategies for the management of dental dysmorphologies.

RESOURCE AVAILABILITY

Lead contact

Further information and requests for resources should be directed to and will be fulfilled by the lead contact, Andrés Ruiz-Linares (a.ruizlin@ucl.ac.uk).

Materials availability

This study did not generate new materials.

Data and code availability

- Summary statistics obtained here have been deposited to the GWAS Catalog: GCP000906 (https://www.ebi.ac.uk/gwas/) and are publicly available as of the date of publication. Raw genotype or phenotype data cannot be made available due to restrictions imposed by the ethics approval.
- This paper does not report original code.
- Any additional information required to reanalyze the data reported in this paper is available upon request.

ACKNOWLEDGMENTS

We thank the volunteers for their enthusiastic support for this research. We are very grateful to the Universidad de Antioquia School of Dentistry for allowing the use of their facilities for the assessment of volunteers. The Centre de Calcul Intensif d'Aix-Marseille Université is acknowledged for granting access to its high-performance computing resources. The GISMO platform and their staff (University of Burgundy) are acknowledged for granting access to their 3D computing resources. We thank the reviewers, Denis Headon and Clément Zanolli, for comments on the manuscript. Work leading to this publication was funded by grants from the National Natural Science Foundation of China (#31771393), the Scientific and Technology Committee of Shanghai Municipality (18490750300), Ministry of Science and Technology of China (2020YFE0201600), Shanghai Municipal Science and Technology Major Project (2017SHZDZX01), the 111 Project (B13016), the Leverhulme Trust (F/07 134/DF), BBSRC (BB/I021213/1), the Excellence Initiative of Aix-Marseille University - A*MIDEX (a French "Investissements d'Avenir" programme), the National Natural Science Founddation of China (#31771393), Universidad de Antioquia (CODI sostenibilidad de grupos 2013–2014 and MASO 2013–2014), Wenner-Gren Foundation for Anthropological Research grant/award number 9391, Universidad de Antioquia grant/award CODI 2014-1124, and a Stowers Family Endowment.

AUTHOR CONTRIBUTIONS

Conceptualization, K.A., M.D., and A.R.-L.; formal analysis, J.C., T.C.C., M.D., P.F., M.P.H., Q.L., N.N., V.P., E.W.W., and Y.Z.; data curation, V.A., M.-C.B., Y.C., L.D., M.D., M.F.-G., C.G., R.G.-J., C.P., G.P., L.P., F.R., L.M.R., W.R., E.S., E.W.W., and G.Y.; writing – original draft, T.C.C., P.F., Q.L., N.N., and A.R.-L.; writing – review & editing, K.A., M.D., and A.R.-L.; supervision, A.R.-L.; funding acquisition, T.C.C., M.D., N.N., and A.R.-L.

DECLARATION OF INTERESTS

The authors declare no competing interests.

STAR★METHODS

Detailed methods are provided in the online version of this paper and include the following:

SUPPLEMENTAL INFORMATION

Supplemental information can be found online at https://doi.org/10.1016/j.cub.2024.11.027.

Received: May 31, 2024
Revised: September 29, 2024
Accepted: November 15, 2024
Published: December 12, 2024

REFERENCES

1. Scott, G.R., Christy, G., Turner, I.I., Townsend, G.C., and Martinon-Torres, M. (2018). The Anthropology of Modern Human Teeth. Dental Morphology and Its Variation in Recent and Fossil Homo sapiens (Cambridge University Press).
2. Rathmann, H., Perretti, S., Porcu, V., Hanihara, T., Scott, G.R., Irish, J.D., Reyes-Centeno, H., Ghirotto, S., and Harvati, K. (2023). Inferring human neutral genetic variation from craniodental phenotypes. PNAS Nexus *2*, pgad217. https://doi.org/10.1093/pnasnexus/pgad217.
3. Dempsey, P.J., and Townsend, G.C. (2001). Genetic and environmental contributions to variation in human tooth size. Heredity *86*, 685–693. https://doi.org/10.1046/j.1365-2540.2001.t01-1-00878.x.
4. Stojanowski, C.M., Paul, K.S., Seidel, A.C., Duncan, W.N., and Guatelli-Steinberg, D. (2017). Heritability and genetic integration of tooth size in the South Carolina Gullah. American Journal of Physical Anthropology *164*, 505–521. https://doi.org/10.1002/ajpa.23290.
5. Nitayavardhana, I., Theerapanon, T., Srichomthong, C., Piwluang, S., Wichadakul, D., Porntaveetus, T., and Shotelersuk, V. (2020). Four novel mutations of FAM20A in amelogenesis imperfecta type IG and review of literature for its genotype and phenotype spectra. Mol. Genet. Genomics *295*, 923–931. https://doi.org/10.1007/s00438-020-01668-8.
6. Kimura, R., Yamaguchi, T., Takeda, M., Kondo, O., Toma, T., Haneji, K., Hanihara, T., Matsukusa, H., Kawamura, S., Maki, K., et al. (2009). A Common Variation in EDAR Is a Genetic Determinant of Shovel-Shaped Incisors. Am. J. Hum. Genet. *85*, 528–535. https://doi.org/10.1016/j.ajhg.2009.09.006.
7. Kimura, R., Watanabe, C., Kawaguchi, A., Kim, Y.-I., Park, S.-B., Maki, K., Ishida, H., and Yamaguchi, T. (2015). Common polymorphisms in WNT10A affect tooth morphology as well as hair shape. Hum. Mol. Genet. *24*, 2673–2680. https://doi.org/10.1093/hmg/ddv014.
8. Tam, V., Patel, N., Turcotte, M., Bossé, Y., Paré, G., and Meyre, D. (2019). Benefits and limitations of genome-wide association studies. Nat. Rev. Genet. *20*, 467–484. https://doi.org/10.1038/s41576-019-0127-1.
9. Küchler, E.C., Kirschneck, C., Marañón-Vásquez, G.A., Schroder, Â.G.D., Baratto-Filho, F., Romano, F.L., Stuani, M.B.S., Matsumoto, M.A.N., and de Araujo, C.M. (2024). Mandibular and dental measurements for sex determination using machine learning. Sci. Rep. *14*, 9587. https://doi.org/10.1038/s41598-024-59556-9.
10. Hanihara, T., and Ishida, H. (2005). Metric dental variation of major human populations. Am. J. Phys. Anthropol. *128*, 287–298. https://doi.org/10.1002/ajpa.20080.
11. Svenson, K.L., Gatti, D.M., Valdar, W., Welsh, C.E., Cheng, R., Chesler, E.J., Palmer, A.A., McMillan, L., and Churchill, G.A. (2012). High-resolution genetic mapping using the Mouse Diversity outbred population. Genetics *190*, 437–447. https://doi.org/10.1534/genetics.111.132597.
12. Katz, D.C., Aponte, J.D., Liu, W., Green, R.M., Mayeux, J.M., Pollard, K.M., Pomp, D., Munger, S.C., Murray, S.A., Roseman, C.C., et al. (2020). Facial shape and allometry quantitative trait locus intervals in the

Diversity Outbred mouse are enriched for known skeletal and facial development genes. PLoS One *15*, e0233377. https://doi.org/10.1371/journal.pone.0233377.

13. Bonfante, B., Faux, P., Navarro, N., Mendoza-Revilla, J., Dubied, M., Montillot, C., Wentworth, E., Poloni, L., Varón-González, C., Jones, P., et al. (2021). A GWAS in Latin Americans identifies novel face shape loci, implicating VPS13B and a Denisovan introgressed region in facial variation. Sci. Adv. *7*, eabc6160. https://doi.org/10.1126/sciadv.abc6160.
14. Li, Q., Chen, J., Faux, P., Delgado, M.E., Bonfante, B., Fuentes-Guajardo, M., Mendoza-Revilla, J., Chacón-Duque, J.C., Hurtado, M., Villegas, V., et al. (2023). Automatic landmarking identifies new loci associated with face morphology and implicates Neanderthal introgression in human nasal shape. Commun. Biol. *6*, 481. https://doi.org/10.1038/s42003-023-04838-7.
15. Zhang, M.F., Wu, S.J., Du, S.Y., Qian, W., Chen, J.Y., Qiao, L., Yang, Y.J., Tan, J.Z., Yuan, Z.Y., Peng, Q.Q., et al. (2022). Genetic variants underlying differences in facial morphology in East Asian and European populations. Nat. Genet. *54*, 403–411. https://doi.org/10.1038/s41588-022-01038-7.
16. Gage, P.J., Suh, H., and Camper, S.A. (1999). Dosage requirement of Pitx2 for development of multiple organs. Development *126*, 4643–4651. https://doi.org/10.1242/dev.126.20.4643.
17. Winchester, E.W., Hardy, A., and Cotney, J. (2022). Integration of multimodal data in the developing tooth reveals candidate regulatory loci driving human odontogenic phenotypes. Front. Dent. Med. *3*, 1009264. https://doi.org/10.3389/fdmed.2022.1009264.
18. Thesleff, I., Keränen, S., and Jernvall, J. (2001). Enamel Knots as Signaling Centers Linking Tooth Morphogenesis and Odontoblast Differentiation. Adv. Dent. Res. *15*, 14–18. https://doi.org/10.1177/089593740101500104 01.
19. Lu, M.F., Pressman, C., Dyer, R., Johnson, R.L., and Martin, J.F. (1999). Function of Rieger syndrome gene in left-right asymmetry and craniofacial development. Nature *401*, 276–278. https://doi.org/10.1038/45797.
20. Vernot, B., and Akey, J.M. (2014). Resurrecting surviving Neandertal lineages from modern human genomes. Science *343*, 1017–1021. https://doi.org/10.1126/science.1245938.
21. Chen, L., Wolf, A.B., Fu, W., Li, L., and Akey, J.M. (2020). Identifying and Interpreting Apparent Neanderthal Ancestry in African Individuals. Cell *180*, 677–687.e16. https://doi.org/10.1016/j.cell.2020.01.012.
22. Popowics, T., and Mulimani, P. (2023). Mammalian dental diversity: an evolutionary template for regenerative dentistry. Front. Dent. Med. *4*, 1158482. https://doi.org/10.3389/fdmed.2023.1158482.
23. Freeman, P.W. (2011). Ungar, Peter S. 2010. Mammalian Teeth: Origin, Evolution, and Diversity. The Johns Hopkins University Press-Baltimore, Maryland, 304 pp. ISBN-13: 978-0-8018–9668-2, price (hardbound), $95.00. J. Mammal. *92*, 1138–1140. https://doi.org/10.1093/jmammal/92.5.1138.
24. Horvath, J.E., Ramachandran, G.L., Fedrigo, O., Nielsen, W.J., Babbitt, C.C., St Clair, E.M., Pfefferle, L.W., Jernvall, J., Wray, G.A., and Wall, C.E. (2014). Genetic comparisons yield insight into the evolution of enamel thickness during human evolution. J. Hum. Evol. *73*, 75–87. https://doi.org/10.1016/j.jhevol.2014.01.005.
25. Mu, Y., Tian, R., Xiao, L., Sun, D., Zhang, Z., Xu, S., and Yang, G. (2021). Molecular Evolution of Tooth-Related Genes Provides New Insights into Dietary Adaptations of Mammals. J. Mol. Evol. *89*, 458–471. https://doi.org/10.1007/s00239-021-10017-1.
26. Martin, R.M.G., Hublin, J.J., Gunz, P., and Skinner, M.M. (2017). The morphology of the enamel-dentine junction in Neanderthal molars: Gross morphology, non-metric traits, and temporal trends. J. Hum. Evol. *103*, 20–44. https://doi.org/10.1016/j.jhevol.2016.12.004.
27. Delezene, L.K., and Ungar, P.S. (2018). Hominin dental evolution. In The International Encyclopedia of Biological Anthropology, pp. 1–10. https://doi.org/10.1002/9781118584538.ieba0123.
28. Bryk, J., Hardouin, E., Pugach, I., Hughes, D., Strotmann, R., Stoneking, M., and Myles, S. (2008). Positive Selection in East Asians for an EDAR Allele that Enhances NF-κB Activation. PLoS One *3*, e2209. https://doi.org/10.1371/journal.pone.0002209.
29. Sabeti, P.C., Varilly, P., Fry, B., Lohmueller, J., Hostetter, E., Cotsapas, C., Xie, X., Byrne, E.H., McCarroll, S.A., Gaudet, R., et al. (2007). Genome-wide detection and characterization of positive selection in human populations. Nature *449*, 913–918. https://doi.org/10.1038/nature06250.
30. Adhikari, K., Fontanil, T., Cal, S., Mendoza-Revilla, J., Fuentes-Guajardo, M., Chacón-Duque, J.C., Al-Saadi, F., Johansson, J.A., Quinto-Sanchez, M., Acuña-Alonzo, V., et al. (2016). A genome-wide association scan in admixed Latin Americans identifies loci influencing facial and scalp hair features. Nat. Commun. *7*, 10815. https://doi.org/10.1038/ncomms10815.
31. Adhikari, K., Fuentes-Guajardo, M., Quinto-Sánchez, M., Mendoza-Revilla, J., Camilo Chacón-Duque, J., Acuña-Alonzo, V., Jaramillo, C., Arias, W., Lozano, R.B., Pérez, G.M., et al. (2016). A genome-wide association scan implicates DCHS2, RUNX2, GLI3, PAX1 and EDAR in human facial variation. Nat. Commun. *7*, 11616. https://doi.org/10.1038/ncomms11616.
32. Adhikari, K., Reales, G., Smith, A.J.P., Konka, E., Palmen, J., Quinto-Sanchez, M., Acuña-Alonzo, V., Jaramillo, C., Arias, W., Fuentes, M., et al. (2015). A genome-wide association study identifies multiple loci for variation in human ear morphology. Nat. Commun. *6*, 7500. https://doi.org/10.1038/ncomms8500.
33. Zhang, L., Yu, M., Wong, S.-W., Qu, H., Cai, T., Liu, Y., Liu, H., Fan, Z., Zheng, J., Zhou, Y., et al. (2020). Comparative analysis of rare EDAR mutations and tooth agenesis pattern in EDAR- and EDA-associated nonsyndromic oligodontia. Hum. Mutat. *41*, 1957–1966. https://doi.org/10.1002/humu.24104.
34. Charles, C., Pantalacci, S., Tafforeau, P., Headon, D., Laudet, V., and Viriot, L. (2009). Distinct impacts of Eda and Edar loss of function on the mouse dentition. PLoS One *4*, e4985. https://doi.org/10.1371/journal.pone.0004985.
35. Kavanagh, K.D., Evans, A.R., and Jernvall, J. (2007). Predicting evolutionary patterns of mammalian teeth from development. Nature *449*, 427–432. https://doi.org/10.1038/nature06153.
36. Sadier, A., Twarogowska, M., Steklikova, K., Hayden, L., Lambert, A., Schneider, P., Laudet, V., Hovorakova, M., Calvez, V., and Pantalacci, S. (2019). Modeling Edar expression reveals the hidden dynamics of tooth signaling center patterning. PLoS Biol. *17*, e3000064. https://doi.org/10.1371/journal.pbio.3000064.
37. Sadier, A., Santana, S.E., and Sears, K.E. (2020). The role of core and variable Gene Regulatory Network modules in tooth development and evolution.. Published online August 6, 2020. Integr. Comp. Biol. https://doi.org/10.1093/icb/icaa116.
38. Tran, T.Q., and Kioussi, C. (2021). Pitx genes in development and disease. Cell. Mol. Life Sci. *78*, 4921–4938. https://doi.org/10.1007/s00018-021-03833-7.
39. Yu, W., Sun, Z., Sweat, Y., Sweat, M., Venugopalan, S.R., Eliason, S., Cao, H., Paine, M.L., and Amendt, B.A. (2020). Pitx2-Sox2-Lef1 interactions specify progenitor oral/dental epithelial cell signaling centers. Development *147*, dev186023. https://doi.org/10.1242/dev.186023.
40. Arte, S., Pöyhönen, M., Myllymäki, E., Ronkainen, E., Rice, D.P., and Nieminen, P. (2023). Craniofacial and dental features of Axenfeld-Rieger syndrome patients with PITX2 mutations. Orthod. Craniofac. Res. *26*, 320–330. https://doi.org/10.1111/ocr.12631.
41. Hermans, F., Hemeryck, L., Lambrichts, I., Bronckaers, A., and Vankelecom, H. (2021). Intertwined Signaling Pathways Governing Tooth Development: A Give-and-Take Between Canonical Wnt and Shh. Front. Cell Dev. Biol. *9*, 758203. https://doi.org/10.3389/fcell.2021.758203.
42. Patel, V.N., Pineda, D.L., Berenstein, E., Hauser, B.R., Choi, S., Prochazkova, M., Zheng, C., Goldsmith, C.M., van Kuppevelt, T.H., Kulkarni, A., et al. (2021). Loss of Hs3st3a1 or Hs3st3b1 enzymes alters heparan sulfate to reduce epithelial morphogenesis and adult salivary gland function. Matrix Biol. *103–104*, 37–57. https://doi.org/10.1016/j.matbio.2021.10.002.

43. Trakinienė, G., Šidlauskas, A., Trakinis, T., Andriuškevičiūtė, I., and Šalomskienė, L. (2018). The Impact of Genetics and Environmental Factors on the Position of the Upper Third Molars. J. Oral Maxillofac. Surg. *76*, 2271–2279. https://doi.org/10.1016/j.joms.2018.05.005.

44. Gkantidis, N., Tacchi, M., Oeschger, E.S., Halazonetis, D., and Kanavakis, G. (2021). Third Molar Agenesis Is Associated with Facial Size. Biology *10*, 650. https://doi.org/10.3390/biology10070650.

45. Li, X., Venugopalan, S.R., Cao, H., Pinho, F.O., Paine, M.L., Snead, M.L., Semina, E.V., and Amendt, B.A. (2014). A model for the molecular underpinnings of tooth defects in Axenfeld-Rieger syndrome. Hum. Mol. Genet. *23*, 194–208. https://doi.org/10.1093/hmg/ddt411.

46. Wang, Z., Patel, V.N., Song, X., Xu, Y., Kaminski, A.M., Doan, V.U., Su, G., Liao, Y., Mah, D., Zhang, F., et al. (2023). Increased 3-O-sulfated heparan sulfate in Alzheimer's disease brain is associated with genetic risk gene HS3ST1. Sci. Adv. *9*, eadf6232. https://doi.org/10.1126/sciadv.adf6232.

47. Xu, X., Liu, C., and Zheng, Y. (2019). 3D Tooth Segmentation and Labeling Using Deep Convolutional Neural Networks. IEEE Trans. Vis. Comput. Graph. *25*, 2336–2348. https://doi.org/10.1109/TVCG.2018.2839685.

48. O'Connell, J., Gurdasani, D., Delaneau, O., Pirastu, N., Ulivi, S., Cocca, M., Traglia, M., Huang, J., Huffman, J.E., Rudan, I., et al. (2014). A General Approach for Haplotype Phasing across the Full Spectrum of Relatedness. PLoS Genet. *10*, e1004234. https://doi.org/10.1371/journal.pgen.1004234.

49. Howie, B., Fuchsberger, C., Stephens, M., Marchini, J., and Abecasis, G.R. (2012). Fast and accurate genotype imputation in genome-wide association studies through pre-phasing. Nat. Genet. *44*, 955–959. https://doi.org/10.1038/ng.2354.

50. Rolfe, S., Pieper, S., Porto, A., Diamond, K., Winchester, J., Shan, S., Kirveslahti, H., Boyer, D., Summers, A., and Maga, A.M. (2021). SlicerMorph: An open and extensible platform to retrieve, visualize and analyse 3D morphology. Methods Ecol. Evol. *12*, 1816–1825. https://doi.org/10.1111/2041-210X.13669.

51. Avants, B.B., Tustison, N.J., Song, G., Cook, P.A., Klein, A., and Gee, J.C. (2011). A reproducible evaluation of ANTs similarity metric performance in brain image registration. NeuroImage *54*, 2033–2044. https://doi.org/10.1016/j.neuroimage.2010.09.025.

52. Schlager, S. (2017). Morpho and Rvcg – Shape Analysis in {R} (Academic Press).

53. Myronenko, A., and Song, X. (2010). Point set registration: coherent point drift. IEEE Trans. Pattern Anal. Mach. Intell. *32*, 2262–2275. https://doi.org/10.1109/TPAMI.2010.46.

54. Porto, A., Rolfe, S., and Maga, A.M. (2021). ALPACA: A fast and accurate computer vision approach for automated landmarking of three-dimensional biological structures. Methods Ecol. Evol. *12*, 2129–2144. https://doi.org/10.1111/2041-210X.13689.

55. Broman, K.W., Gatti, D.M., Simecek, P., Furlotte, N.A., Prins, P., Sen, Ś., Yandell, B.S., and Churchill, G.A. (2019). R/qtl2: Software for Mapping Quantitative Trait Loci with High-Dimensional Data and Multiparent Populations. Genetics *211*, 495–502. https://doi.org/10.1534/genetics.118.301595.

56. Yang, J., Zaitlen, N.A., Goddard, M.E., Visscher, P.M., and Price, A.L. (2014). Advantages and pitfalls in the application of mixed-model association methods. Nat. Genet. *46*, 100–106. https://doi.org/10.1038/ng.2876.

57. x, Genomics.. Nuclei Isolation from Embryonic Mouse Brain for Single Cell Multiome ATAC + Gene Expression Sequencing. https://www.10xgenomics.com/support/single-cell-multiome-atac-plus-gene-expression/documentation/steps/sample-prep/nuclei-isolation-from-embryonic-mouse-brain-tissue-for-single-cell-multiome-atac-plus-gene-expression-sequencing.

58. Granja, J.M., Corces, M.R., Pierce, S.E., Bagdatli, S.T., Choudhry, H., Chang, H.Y., and Greenleaf, W.J. (2021). ArchR is a scalable software package for integrative single-cell chromatin accessibility analysis. Nat. Genet. *53*, 403–411. https://doi.org/10.1038/s41588-021-00790-6.

59. Nasser, J., Bergman, D.T., Fulco, C.P., Guckelberger, P., Doughty, B.R., Patwardhan, T.A., Jones, T.R., Nguyen, T.H., Ulirsch, J.C., Lekschas, F., et al. (2021). Genome-wide enhancer maps link risk variants to disease genes. Nature *593*, 238–243. https://doi.org/10.1038/s41586-021-03446-x.

60. Limaye, A. (2012). Drishti: a Volume Exploration and Presentation Tool (SPIE). https://doi.org/10.1117/12.935640.

61. Goedhart, J. (2021). SuperPlotsOfData-a web app for the transparent display and quantitative comparison of continuous data from different conditions. Mol. Biol. Cell *32*, 470–474. https://doi.org/10.1091/mbc.E20-09-0583.

62. Alexander, D.H., Novembre, J., and Lange, K. (2009). Fast model-based estimation of ancestry in unrelated individuals. Genome Res. *19*, 1655–1664. https://doi.org/10.1101/gr.094052.109.

63. Chacón-Duque, J.C., Adhikari, K., Fuentes-Guajardo, M., Mendoza-Revilla, J., Acuña-Alonzo, V., Barquera, R., Quinto-Sánchez, M., Gómez-Valdés, J., Everardo-Martínez, P., Villamil-Ramírez, H., et al. (2018). Latin Americans show wide-spread Converso ancestry and imprint of local Native ancestry on physical appearance. Nat. Commun. *9*, 5388. https://doi.org/10.1038/s41467-018-07748-z.

64. Manichaikul, A., Mychaleckyj, J.C., Rich, S.S., Daly, K., Sale, M., and Chen, W.M. (2010). Robust relationship inference in genome-wide association studies. Bioinformatics *26*, 2867–2873. https://doi.org/10.1093/bioinformatics/btq559.

65. MacKinnon, D.P., Lockwood, C.M., Hoffman, J.M., West, S.G., and Sheets, V. (2002). A comparison of methods to test mediation and other intervening variable effects. Psychol. Methods *7*, 83–104. https://doi.org/10.1037/1082-989x.7.1.83.

66. Tingley, D., Yamamoto, T., Hirose, K., Keele, L., and Imai, K. (2013). mediation: R Package for Causal Mediation Analysis. J. Stat. Softw. *59*, 1–38.

67. Paria, S.S., Rahman, S.R., and Adhikari, K. (2022). fastman: A fast algorithm for visualizing GWAS results using Manhattan and Q-Q plots. Preprint at bioRxiv. https://doi.org/10.1101/2022.04.19.488738.

68. Li, J., and Ji, L. (2005). Adjusting multiple testing in multilocus analyses using the eigenvalues of a correlation matrix. Heredity (Edinb) *95*, 221–227. https://doi.org/10.1038/sj.hdy.6800717.

69. Racimo, F., Gokhman, D., Fumagalli, M., Ko, A., Hansen, T., Moltke, I., Albrechtsen, A., Carmel, L., Huerta-Sánchez, E., and Nielsen, R. (2017). Archaic Adaptive Introgression in TBX15/WARS2. Mol. Biol. Evol. *34*, 509–524. https://doi.org/10.1093/molbev/msw283.

70. Delaneau, O., Zagury, J.F., Robinson, M.R., Marchini, J.L., and Dermitzakis, E.T. (2019). Accurate, scalable and integrative haplotype estimation. Nat. Commun. *10*, 5436. https://doi.org/10.1038/s41467-019-13225-y.

71. Prüfer, K., de Filippo, C., Grote, S., Mafessoni, F., Korlević, P., Hajdinjak, M., Vernot, B., Skov, L., Hsieh, P., Peyrégne, S., et al. (2017). A high-coverage Neandertal genome from Vindija Cave in Croatia. Science *358*, 655–658. https://doi.org/10.1126/science.aao1887.

72. Sudmant, P.H., Rausch, T., Gardner, E.J., Handsaker, R.E., Abyzov, A., Huddleston, J., Zhang, Y., Ye, K., Jun, G., Fritz, M.H.Y., et al. (2015). An integrated map of structural variation in 2,504 human genomes. Nature *526*, 75–81. https://doi.org/10.1038/nature15394.

73. Faux, P., Ding, L., Ramirez-Aristeguieta, L.M., Chacón-Duque, J.C., Comini, M., Mendoza-Revilla, J., Fuentes-Guajardo, M., Jaramillo, C., Arias, W., Hurtado, M., et al. (2023). Neanderthal introgression in SCN9A impacts mechanical pain sensitivity. Commun. Biol. *6*, 958. https://doi.org/10.1038/s42003-023-05286-z.

74. Maples, B.K., Gravel, S., Kenny, E.E., and Bustamante, C.D. (2013). RFMix: a discriminative modeling approach for rapid and robust local-ancestry inference. Am. J. Hum. Genet. *93*, 278–288. https://doi.org/10.1016/j.ajhg.2013.06.020.

75. Delaneau, O., Zagury, J.F., and Marchini, J. (2013). Improved whole-chromosome phasing for disease and population genetic studies. Nat. Methods *10*, 5–6. https://doi.org/10.1038/nmeth.2307.

STAR★METHODS

KEY RESOURCES TABLE

REAGENT or RESOURCE	SOURCE	IDENTIFIER
Deposited data		
Genome-wide association scan summary data	This paper	GWAS Catalog: GCP000906
Micro-computed tomography (microCT) head and genotypes of 1,147 Diversity Outbred mice	FaceBase consortium website	www.facebase.org
Experimental models: Organisms/strains		
Mouse: Pitx2-Cre knock-in driver line	Professor James Martin (Baylor College of Medicine, Texas)	https://doi.org/10.1038/45797
Mouse: Hs3st3a1;Hs3st3b1 DKO	Professor Matthew P. Hoffman	https://doi.org/10.1126/sciadv.adf6232
Software and algorithms		
Dental arcade segmentation algorithms	Professor Youyi Zheng (https://doi.org/10.1109/TVCG.2018.2839685)	N/A
PLINK v1.90	https://www.cog-genomics.org/plink/1.9	N/A
SHAPEIT2	https://mathgen.stats.ox.ac.uk/genetics_software/shapeit/shapeit.html	N/A
IMPUTE2	https://mathgen.stats.ox.ac.uk/impute/impute_v2.html	N/A
Fastman	https://www.biorxiv.org/content/10.1101/2022.04.19.488738v1 https://github.com/kaustubhad/fastman	N/A
SlicerMorph	https://slicermorph.github.io/	N/A
ANTsRCore package	https://github.com/ANTsX/ANTsRCore	N/A
Rvcg package	https://cloud.r-project.org/web/packages/Rvcg	N/A
qtl2 package	https://github.com/rqtl/qtl2	N/A
ArchR (v.1.0.1)	https://github.com/GreenleafLab/ArchR/releases	N/A
SuperPlotsOfData	https://github.com/JoachimGoedhart/SuperPlotsOfData	N/A
Onewaytests package	https://journal.r-project.org/articles/RJ-2018-022/	N/A
ADMIXTURE	http://dalexander.github.io/admixture/	N/A
ppcor package	https://cran.r-project.org/web//packages/ppcor/	N/A
KING-robust	https://www.kingrelatedness.com/	N/A
admixtureHMM	https://github.com/amyko/admixtureHMM	N/A
Shapeit4	https://odelaneau.github.io/shapeit4/	N/A
RFMix v1	https://github.com/indraniel/rfmix	N/A

EXPERIMENTAL MODELS AND STUDY PARTICIPANTS

Human subjects

Our study sample consists of cohorts of individuals recruited in Medellín, Colombia (mostly students and staff of Universidad de Antioquia). One set consisted of 316 individuals from the CANDELA cohort[13,30–32] who we recontacted for this study. The second set consisted of 566 individuals recruited specifically for this study but using the same approach as for the CANDELA cohort. The full study sample included 882 individuals (54% women), aged 18–40 years (mean = 22.9). Stature information was available for 743 of these individuals. For replication analyses, we recruited a second cohort in Arica, Chile, comprising 186 individuals (67% women), aged 18–45 years (mean = 33.0). Recruitment was carried out with the approval of the ethics committees of Universidad de Antioquia (Medellín, Colombia) or Universidad de Tarapacá (Arica, Chile). All participants provided written informed consent.

Mutant animals

The *Pitx2-Cre* knock-in driver line, which is haplo-insufficient for *Pitx2* due to the insertional inactivation by Cre integration, was previously described[45] and was a kind gift from Professor James Martin (Baylor College of Medicine, Texas). Hereafter, these mice are referred to as *Pitx2* heterozygotes and were maintained under a protocol (#41143) approved by the University of Missouri-Kansas City's Animal Care and Use Committee. *Hs3st3a1* and *Hs3st3b1* encode paralogous heparan sulphate sulfotransferases that are members of a larger family of sulfotransferase that exhibit some functional redundancy.[42] The generation of the *Hs3st3a1* and *Hs3st3b1* double knockout mice (*Hs3st3a1;Hs3st3b1* DKO) has previously been described and are viable and fertile.[46] All mice were maintained on a C57BL/6J background and treated according to guidelines approved by the National Institute of Dental and Craniofacial Research and National Institutes of Health Animal Care and Use Committee (protocol number ASP-20-1048). Information on sex, genotype, and developmental stage is provided in the subsequent section.

METHOD DETAILS

Phenotyping

Dental plaster casts were obtained using alginate (hydrogum fast setting elastic alginate - Zhermack) and gypsum (elite ortho white - Zhermack) materials. The dental casts were scanned using a DAVID SLS-2 structured light 3Dscanner (DAVID Vision Systems, Koblenz, Germany) or a portable 3D Artec Space Spider scanner (Artec 3D, Santa Clara, California). High resolution 3D models were then exported as stereo-lithography (STL) files, including volume, color and texture. Individual teeth were extracted from the 3D models of each dental arcade using an automatic segmentation approach.[47]

To orientate each tooth consistently, we obtained a rotation matrix and applied it to their original location on the dental arcade (Figure 1). The accuracy of the automatic segmentation and orientation procedure was evaluated manually by visualizing the results using a custom R script (Figure 1). Cases with segmentation or orientation problems were excluded from the subsequent analysis. After alignment, individual tooth measurements were obtained automatically by calculating the difference between the maximum and minimum coordinates of a mesh vertex along each axis: mesiodistal diameter (MDD, x-axis), buccolingual diameter (BLD, y-axis), and height (H, z-axis), respectively. Specifically, MDD is the distance between the most mesial (toward the midline of the dental arch) and the most distal (away from the midline of the dental arch) points of the tooth, measured along the x-axis. BLD is the distance between the most buccal (toward the cheek) and the most lingual (toward the tongue) points of the tooth, measured along the y-axis. H is the distance from the highest point of the tooth crown to the lowest point of the tooth crown, measured along the z-axis. The measurements were extracted using a custom R script that processed the 3D coordinates of the mesh vertices.

The crown measurements we obtained are not identical to the definitions of crown MDD, BLD and H in dental anthropology. Particularly, H is usually defined as the distance between the top of the crown and the enamel-cementum junction. Rather, our measurement of H corresponds to ''clinical crown height'' as defined by the World Dental Federation: the distance between the highest point on the tooth crown to the lowest edge of the gum.

We obtained these measurements for all available first and second incisors (I1 and I2), canines (C), first and second premolars (P1 and P2) and first and second molars (M1 and M2) of upper (U) and lower (L) teeth on both the left (L) and right (R) sides of the dental arcades. Third molars were not considered as they were missing in most individuals. For the subsequent analyses we excluded measurements exceeding +/- three standard deviations from the mean. This step was performed separately for men and women. The final sample size for each measurement ranged between 610-720 in the Colombian sample and 123-146 in the Chilean sample.

Genotype data

DNA extraction (from blood or saliva) and genotyping followed standard laboratory protocols. The first set of 316 CANDELA Colombian individuals were previously genotyped on Illumina's HumanOmniExpress chip.[13,30–32] The second set of 566 Colombians and the 186 Chileans were genotyped on Illumina's HumanOmniExpress or GSA chips. Of the 566 Colombian samples, 156 were genotyped on the HumanOmniExpress chip, and 410 on the GSA chip. All 186 Chilean samples were genotyped on the GSA chip. Thus, in total, 472 individuals (all Colombians) were genotyped on the HumanOmniExpress chip and 596 individuals (Colombians and Chileans) on the GSA chip. PLINK v1.90 was used for quality control of genotyping data. Individuals and SNPs with >5% missing genotypes, SNPs with <5% minor allele frequency (MAF), and individuals who failed the X- or Y- chromosome sex checks were excluded. After these QC filters, 697,067 variants for the Illumina HumanOmniExpress chip and 683,494 variants for the Illumina GSA chip were retained for further analyses.

Prior to imputation, we assessed the potential batch effect between genotyping chips. We first merged the genotypes of the two genotyping chips (Illumina GSA and Illumina OmniExpress) over the 181,667 autosomal variants common to both chips and with MAF>1%. Then, we computed the top ten principal components (PCs) and, for each of those, tested whether the means of individuals of each chip were different or not. The top PCs capture the main population structure (e.g. continental ancestry clines) and, although individuals from the two genotyping chips show overlapping clouds, they two batches have slightly different ancestry compositions (see Figure S6) due to the urban sampling location being very ethnically diverse and admixed. Therefore, we have adjusted the PCs to the three main ancestries (African, European and Native American) before testing mean differences. The tests results are shown in Table S6: accounting for multiple testing (significant if $p < 0.005$), none of the top-ten PCs have a significantly different mean across genotyping chips, indicating thereby that no potential batch effect was detected.

Imputation was performed separately for the HumanOmniExpress and GSA datasets but using the same approach. First, SHAPEIT2[48] was used with default parameters to pre-phase the chip data. IMPUTE2[49] was then used to impute variants using the 2,504 individuals from the 1000GP3 as reference. Eventually, in each separate set, we retained only the variants with high genotype reliability, those complying with the following conditions: (i) imputation quality scores (INFO scores) equal or above 0.40, (ii) concordance value above 0.70, (iii) gap between the INFO score and concordance value below or equal to 0.10, (iv) call rate equal or above 0.95 after marking individual genotypes with maximum genotype probability below 0.90 as missing and (v) minor allelic frequency above 0.01. These filtering rules led to similar numbers of retained variants for both sets: 11,532,785 SNPs for the set using the HumanOmniExpress chip, and 11,632,267 SNPs for the set using the GSA chip. Among them, 11,027,943 variants were retained in both datasets.

To further filter-out potentially misimputed SNPs, we discarded 730 SNPs (0.007% of the total) whose reference allelic frequency in each set differed by >0.20. The remaining SNPs were merged into a single dataset, from which we further filtered-out: (i) SNPs within segments of low confidence in local ancestry (29 segments covering 71.3Mb, see below), and (ii) SNPs with >5% missingness or with MAF<5% in the study sample. The final merged dataset used in the analyses included 6,332,275 genotyped or imputed SNPs.

Outbred mice analyses

A sample of 1,147 Diversity Outbred (DO) mice was used for QTL analysis. DO is a heterogeneous stock derived from the intercrossing of eight inbred founders[11] over 9 to 27 generations. Micro-computed tomography (microCT) head stacks at voxel sizes of 0.035 mm and genotypes of 56,885 SNPs were retrieved from the FaceBase consortium website (www.facebase.org),[12] corresponding to the "Facial shape and allometry quantitative trait loci in the Diversity Outbred mouse" dataset.[12] The data were downloaded in March 2021 and for 70% of the image stacks on June 20th 2022. Original metadata of microCT and genotyping information can be found in Katz et al.[12]

Registration of image stacks

Global alignment of the image stacks was based on rigid alignment of low-resolution 3D skull models using RANSAC and Iterative Closest Point algorithms as implemented in SlicerMorph.[50] After this general alignment, upper and lower rows on the same side were first registered together to a reference stack manually labelled using a deformable registration based on cross-correlation metric implemented in the ANTsRCore package.[51] Deformable registration was again performed at the row level to improve correspondence with the reference individual.

All left-side and 50% of right-side molar registrations underwent manual verification, and for a few a manual correction was applied. A machine learning approach based on gray value quartiles was then employed for QC of the remaining.

Linear measurement of molars

A 3D surface was generated for each molar using the marching cubes algorithm implemented in the Rvcg package.[52] On the reference individual, twelve landmarks were placed to approximate the cingulum along the molar row. To predict these landmarks on other samples, the coherent point drift algorithm[53] was employed through the Alpaca module[54] of SlicerMorph.[50] The principal axes of the twelve cingulum landmarks were used to orient the row and projecting all mesh vertices onto the first principal plane. Individual measurements of the second and third molars were obtained directly from this row alignment by computing the differences between the maximum and minimum coordinates along the two axes, whereas for the more elongated first molar the rotation matrix was first optimized to the principal axes of the tooth.

Outlier values for each molar were removed by excluding teeth exceeding the 2.5th upper quantile of the distribution of the Mahalanobis distance around the mean. Mice with measurements available for both left and right sides (ranging from 488 to 635 mice depending on the specific molar) were averaged. In total, between 913 and 1003 mice have measurements for both the length and the width of a molar, with 792 of them having the complete set of 12 measurements.

QTL mapping

A linear mixed model was fitted at each marker with the fixed effect of sex and DO batches, which differ in number of outcrossing generations and age-at-sacrifice. For each marker, we computed genotype probabilities given the observed multipoint marker data and observed founder haplotypes using the qtl2 package,[55] and combined them to get the expected number of alleles inherited from each of the eight founders. An additional random effect of kinship was included in the model. A leave-one-chromosome-out approach was implemented to estimate this kinship to avoid the inclusion of a tested locus, which is known to reduce power.[56] Mouse loci were defined as the location of the highest -$\log_{10}$p value in a region of ± 2Mb window, crossing a threshold of 3.5, and with 1-LOD drop around.

Furthermore, we repeated the outbred mice analyses considering body mass at sacrifice and facial centroid size, to assess the effect of body size. Mass at sacrifice showed no significant effect on tooth dimensions. Facial centroid size (based on 22 facial landmarks) explained a low (average of 3%) but significant fraction of the variance in length/width of molars. We repeated the QTL analyses including body mass or facial CS as a covariate. The results obtained are very similar to those reported in the manuscript, albeit with some drop in significance for certain regions (Table S7). To ensure consistency with the human data, we presented the analyses without adjusting for body mass or facial centroid size.

Comparison to human hits

Human loci on the GRCh37 were converted in mouse GRCm38 locations using LiftOver tool (https://genome.ucsc.edu/cgi-bin/hgLiftOver). These converted locations were then compared to the mouse hits on the basis of their proximity. The false discovery rate (FDR) of these loci was computed as the ratio of the number of times from 100 randomization per traits a locus was exceeding a given threshold in the ± 2Mb neighborhood of the mouse-converted human locus.

Developing mouse incisor cell-type-specific analyses

We isolated cap stage mandibular incisor buds bilaterally from E13.5 mouse embryos (Bl/6 mice), and pooled ~10 tooth buds from mixed sex littermates. With 3 replicates of these samples, we generated single nucleus ATAC-seq and RNA-seq libraries following a published protocol.[57] These libraries were sequenced on an Illumina NovaSeq 6000 and aligned using a standard CellRanger multiome pipeline.[57] Subsequent analyses were performed using ArchR (v.1.0.1),[58] scripts for which can be found detailed on our github (https://github.com/emmawwinchester/Incisor_Multiome). Briefly, cell types were classified based on previously published canonical marker genes (Figure S3).[17] Each cell type had reproducible ATAC peaks called in a pseudobulk manner using Macs2 and pseudobulk gene expression calculated as transcripts per million. After identification of pseudobulk reproducible ATAC peaks and pseudobulk gene counts, we converted these data to the orthologous regions in the human genome (LiftOver on ATAC peaks, minMatch=0.25; 1:1 ortholog table on gene counts). These data were analyzed together with previously published chromosome conformation capture (Hi-C) data from embryonic human craniofacial tissues using the Activity-by-Contact (ABC) model to predict enhancer:gene pairs.[59] Detailed scripts and blacklists can be found at https://github.com/emmawwinchester/Incisor_Multiome.

Mutant mouse analyses

MicroCT and landmark-based measurements

Heads of six month-old *Pitx2* heterozygotes and sex- and background-matched controls, as well as 10-12 week old *Hs3st3a1-b1* DKO mice and their sex- and background-matched controls, were imaged in a Skyscan 1275 microCT (Bruker; Kontich, Belgium). Six female and two male *Pitx2* heterozygotes and eight female and seven male littermate controls were available for imaging and analysis. For *Hs3st3a1-b1* DKO mice, five male mice were imaged along with five male background matches control mice. Scans were performed at 17.63 micron resolution using the settings: 55 kV, 181 μA, 45 ms exposure, 0.5 mm Al filter, 0.3° rotation step, and 4 frame averaging. Raw scan data were reconstructed using the NRecon software (Bruker) with consistent greyscale threshold values for mutants and their matched controls, then the data rendered in 3D using Drishti Volume Exploration software v3.0.[60]

Within Drishti, the following bilateral measurements were taken: the mesiodistal and buccolingual diameters (MDD and BLD, respectively) of the first, second and third maxillary molars, the maxillary and mandibular alveolar lengths (average of left and right side measurements), the total maxillary and mandibular molar row lengths on each side, and the MDD and BLD of each maxillary incisor. The landmarks used for each measurement were placed independently by two researchers (TC, JC) and are shown and described in Figure S7. Because of the inbred nature of the mice, combined with the independent growth of the dentition on each side, the measurements of the left and right-side molar and incisors were considered distinct measures. Only the left and right-side maxillary and mandibular alveolar measurements were averaged. Measurements were graphed using SuperPlotsOfData[61] and statistically analyzed using Welch's t-test.[61] For the analysis of variation, Levene's test was performed, utilizing the R package onewaytests. Differences were considered significant for comparisons yielding $p<0.05$. For the *Pitx2* heterozygotes, there was no significant difference between measurements from the male and female mice and so the data was combined for the final analyses.

QUANTIFICATION AND STATISTICAL ANALYSES

Ancestry estimation

An LD-pruned set of 93,328 autosomal SNPs was used to estimate European, African and Native American ancestry proportions using supervised runs of ADMIXTURE.[62] Reference parental populations included in the ADMIXTURE analyses consisted of Africans and Europeans from 1000 Genomes Phase 3 and selected Native Americans, as described in Chacón-Duque et al.[63]

Correlation analysis

Spearman's correlations were calculated to assess the relationships between measurements of the upper (U) and lower (L) teeth on the left (L) and right (R) sides of the dental arcades (Table S2). Partial correlation analysis was conducted to examine the relationships between dental measurements and covariates, including age, sex, stature, and genome-wide ancestries (Figure S2; Table S3). The pcor function from the R package ppcor was utilized for this analysis.

To assess the reliability of our automatic MDD, BLD and H measurements, we evaluated intraclass correlations with manual measurements obtained on dental plaster casts of 25 individuals. The manual measurements were obtained with a high-precision digital Mitutoyo caliper (MITUTOYO, 0 in to 6 in / 0 to 150 mm range, ±0.001 in accuracy, 4-Way Digital Caliper - 5C668 | 500-171-30 - Grainger). The Intraclass Correlation Coefficients are shown in Table S1).

GWAS analyses

Relatedness between samples was estimated using KING-robust[64] implemented in PLINK v2.0, which is better suited to estimate relatedness in admixed individuals. Only one individual from any related pair (with a threshold of IBD > 0.1, excluding third degree

relatives and higher) was retained. SNPs with minor allele frequency <5% were excluded, leading to 9,383,530 SNPs being tested. Two sets of analyses were performed. Firstly, GWASs were conducted on left/right average MDD, BLD and H measurements for each individual tooth, using PLINK v.1.9.[47] Secondly, multivariate (Wald test) GWASs were conducted (using R) for MDD, BLD and H for each class of teeth (incisors, canines, premolars and molars). This test excludes individuals with any missing data, resulting in a sample size for the Wald GWASs between 570-704. In all the GWAS analyses we incorporated as covariates age, sex and the first 6 genetic PCs. Since we did not have stature information for ~15% of individuals and we observed a significant correlation between stature and BLD for certain teeth, we evaluated the effect on the GWAS of including stature as a covariate.

In the subset of individuals with stature information, we performed GWAS including stature as a covariate, and contrasted the P-values using Q-Q plots to the GWAS results on the same subset of individuals, excluding stature as a covariate. Results (Data S3) showed that the P-values were nearly identical, and genomic inflation factor (lambda) values for all traits were close to 1 (minimum: 0.997, maximum: 1.006). In particular, the main hits were the same in both analyses, with only some variation in the level of statistical significance for some of them.

Furthermore, we performed a statistical sensitivity analysis to assess the extent of the effect stature was exerting on the GWAS results in the subsample. We used mediation analysis,[65] a kind of structural equation modelling (SEM), to assess the 'indirect effect' of stature on the association between a trait and its index SNP. This was done via the 'Judd & Kenny Difference of Coefficients Approach'[65], which compares the SNP's regression coefficient with and without stature in the GWAS regression model, and tests whether they are significantly different. Calculations performed using the "mediation" package in R[66] showed that for all the 13 univariate traits with significant GWAS associations, the test was non-significant (smallest P-value 0.128, Table S8), indicating that body height had no effect on the GWAS results.

Since these analyses did not evidence a significant effect of stature in the GWAS, in the manuscript we present results from the full sample, analyzed without stature as a covariate.

GWAS results were visualized as Manhattan and Q-Q plots, generated with the R package Fastman.[67] The Q-Q plots for all traits showed no sign of inflation, and the genomic inflation factor (lambda) of all traits was close to 1 with the maximum value of 1.03 and median value of 1.01, which indicate that appropriately controls for population stratification had been taken care of.

Accounting for multiple testing

To account for multiple testing in the GWAS, due to the number of phenotypes examined, we estimated the false discovery rate (FDR) using the Benjamini-Hochberg procedure.[68] This resulted in an adjusted genome-wide significance threshold of 1.64×10^{-7} and 1.23×10^{-6}, for the single-trait and multiple-trait (Wald) analyses, respectively.

We evaluated an alternative FDR calculation based on the effective number of independent tests, corresponding to the number of independent phenotypes times the number of independent SNPs.[14,68] An eigenvalue decomposition of the phenotype correlation matrix leads to an estimation of the effective number of independent phenotypes as 33.78. LD pruning of the genotypic data leads to an estimation of 1,346,783 independent SNPs. The effective number of independent tests was thus estimated as 45,494,330, leading to an adjusted genome-wide significance threshold of 1.65×10^{-7}, very similar to the threshold obtained above.

Since the usual GWAS genome-wide significance threshold is more conservative than both the thresholds estimated using the FDR approach, we decided to retain the standard *P*-value of 5×10^{-8} as threshold for genome-wide significance.

Replication analyses

In the Chilean cohort, we tested for replication of association for the index SNPs at the associated regions detected in the GWAS, using the same univariate and multivariate tests as in the GWAS. Significance thresholds were calculated using Benjamini-Hochberg's FDR procedure as 0.0154 and 0.0324, for the univariate and multivariate analyses, respectively.

Neanderthal introgression analyses

We first searched for tracts of Neanderthal introgression in the 18 genome regions that were significantly associated with at least one trait in the GWAS. We used an HMM-based approach (*admixtureHMM*[69]), in which each chromosome (reconstructed using Shapeit4[70] with default parameters) is modelled as a mosaic of haplotypes of Neanderthal or modern human origin. For this, we used the high-coverage Neanderthal genome sequence from the Vindija cave (Vindija33.19[71]) and YRI sequences from the 1000GP3.[72] We performed a stringent filtering of variants over a 1Mb segment centered around the index SNP for each of the 18 regions associated in the GWAS, retaining only biallelic SNP meeting the following criteria: (i) $\geq$ 20x coverage in the archaic genome, (ii) PASS in each VCF (archaic and 1000GP3), (iii) having consistent ancestral allele reported in each VCF, and (iv) having identical polymorphism in each VCF. Tracts were then called over these SNPs by the Viterbi algorithm implemented in *admixtureHMM* and retained only if called with >99% confidence. Called tracts shorter than 25Kb were subsequently discarded, following an assessment of spurious calls previously made on the CANDELA cohort.[73]

We tested for associations to dental phenotypes for the regions where Neanderthal tracts reached a frequency $\geq$1% in the individuals included in the GWAS. For association testing we used an admixture mapping approach.[14,73] In brief, we first recoded the individual SNP genotypes as the number of Neanderthal tracts called at each position (i.e. 0, 1 or 2). Then, we merged as one segment all consecutive SNPs whose genotypes show < 0.1% difference. Following this procedure, we defined a total of 261 Neanderthal segments (across 14/18 regions). These were tested for association with the same phenotypes that had shown association to these

regions in the GWAS and with the same linear regression that had been used for these association (either regular GWAS or Wald test). Test significance was set at the Bonferroni-corrected threshold of 1.9×10^{-4} (<0.05/261).

We performed further analyses in the only region that showed significant association with Neanderthal ancestry (17p12 with BLD of central upper incisors). Firstly, we ascertained the introgression call by running an IBD-based method that does not require a reference for the modern Human genome, IBDmix (Figure S4).[21] The method ran with values of 0.01 and 0.0025 for allele error rate in the archaic genome and maximum allele error rate in the modern genome respectively, over 2,972 sites (selected by applying the accompanying program "generate_gt" on the imputed variants retained for GWAS). Neanderthal tracts inferred were retained if their length was >25 Kb and their SLOD > 3. Secondly, given the admixed nature of our sampling, we sought to infer the continental background (European or Native American) on which these introgression tracts were preferentially found. To that end, we used local ancestry calls: each phased chromosome was inferred as a mosaic of African, European and Native American segments using RFMix v1[74] with 242 reference individuals for each continental ancestry and 1 EM iteration (more details about local ancestry inference are provided in Faux et al.[73]). Among the individuals qualified for the GWAS of BLD UI1 ($N = 714$), we identified a total of 520 chromosomes with a large ancestry segment ($\geq$10Mb) over the GWAS peak: respectively 22, 404 and 94 segments of African, European and American ancestry. Then, we aligned the imputed phases of these chromosomes (pre-phased using Shapeit4[70] – see above) on the phases on which local ancestry was inferred, allowing to assess the proportion of ancestry tracts found on each continental background. This step was achieved using Shapeit2[75] in "call" mode.